N80-23679

NASA Contractor Report 159261

VISUALIZATION OF IMPACT DAMAGE OF COMPOSITE PLATES BY MEANS OF THE MOIRÉ TECHNIQUE

DTIC ELECTED DEC 2 8 1995 S D F

W. G. Knauss, C. D. Babcock,
and H. Chai

19951218 001

DISTRIBUTION STATEMENT H
Approved for public release
Distribution Unlimited

CALIFORNIA INSTITUTE OF TECHNOLOGY
Pasadena, California 91125

NASA Grant NSG-1483
April 1980

National Aeronautics and
Space Administration
Langley Research Center
Hampton, Virginia 23665

DEPARTMENT OF DEFENSE
PLASTICS TECHNICAL EVALUATION CENTER
ARRADCOM, DOVER, N. J. 07801

DTIC QUALITY INSPECTED 1

PLASTEC 21364

TABLE OF CONTENTS

Accesion For
NTIS CRA&I ☑
DTIC TAB ☐
Unannounced ☐
Justification .....
By .....
Distribution /
Availability Codes
Dist | Avail and / or Special
A-1

LIST OF TABLES

ABSTRACT

The results of a program to determine the phenomenological aspects of the propagation damage due to low velocity impact on heavily loaded graphite-epoxy composite laminates are described. The main tool of this investigation is high speed photography coupled with the moiré fringe technique. High speed moiré motion records of the impacted specimens are presented.

The test results provide information on the time scale and sequence of the failure process. While the generation of the initial damage cannot always be separated temporally from the spreading of the damage, the latter takes place on the average with a speed on the order of 200 m/sec.

I. INTRODUCTION

Graphite-fiber reinforced epoxy laminates are lighter than aluminum, but have a load carrying capacity which makes them attractive in strength-critical application. However, this advantage is decreased by their sensitivity to low velocity impact unless the failure mechanism can be understood and controlled (refs. 1-6). A considerable amount of work has been conducted in the past toward this goal in which a post-mortem examination of the damaged structure served as the main tool.

This study takes a rather different approach in which the propagating failure is observed in real time using high speed photography. The purpose of this work is to gain an understanding of the propagation mechanism so that appropriate models of the failure can be formulated. The emphasis is on the propagation and not the initial damage due to the impact itself.

Tests were conducted on graphite-fiber reinforced laminated panels pre-strained in compression to strain values ranging up to 0.0086. The test specimens were damaged by a 1.27 cm diameter aluminum sphere propelled normal to the center of the specimen. The projectile velocities ranged from 29 m/s to 76 m/s. The moiré fringe technique was used with high speed photography to record out-of-plane deformation of the back surface of the impacted plate.

II. EXPERIMENTAL WORK

a) Test Specimens

The test specimens used in this work have the same properties as those used in ref. 1 and were furnished by NASA Langley. The basic laminate properties and the calculated composite stiffnesses are listed in Table I. Several sizes of test specimens were used in the experimental work. They were cut from three lots of panels. The lots are identified for each specimen in the table showing test conditions (Table II).

b) Specimen Holders

Three specimen holders have been designed for three different kinds of specimens employed in this program; namely, the small specimen holder, the partially free-sided specimen holder, and the large specimen holder. Figure 1a shows photographs of the first holder, while fig. 1b-c shows the other two specimen holders.

The upper and lower parts of all specimen holders provided a clamped type support for the test specimens. This was achieved by bonding the upper and lower parts of the test specimen to aluminum plates. The plates contained a 1.0 cm deep grove which was filled with a bonding agent. In the small specimen holder, both sides of the specimen are held by 3 mm wide flat surfaces. The flat surfaces are adjustable along the length of the specimen to insure a close but not binding support of the sides. The side support rigidity is estimated to lie between simply supported and clamped. In the large specimen holder,

the sides of the specimens are held by 0.5 cm radius circular surfaces, so a line contact along the specimen length is presented. In the partially free-sided support, the contact area along the sides is similar to that of the small specimen holder. Figure 2 gives a description of the edge supports for the holders.

In all three specimen holders the strain distribution was found to be quite uniform and no appreciable bending was detected. The difference in the strain across the panels was bounded by $\pm 3\%$.

c) Impact System

The 1.27 cm aluminum ball is accelerated using a simple air gun. This consists of a compressed air reservoir and a solenoid activated valve which separates the reservoir from a 38 cm (15 in.) long barrel. The projectile velocity is controlled by setting the pressure in the reservoir. The velocity is measured using a laser light beam which is interrupted by the projectile at two points 30.5 cm (12 in.) apart. A photodiode senses the light drop as the projectile interrupts the laser beam. The time interval between the two light drops is then determined by a counter from which the projectile velocity can be calculated. The velocity can be controlled and measured to within $\pm 1\%$.

d) High Speed Photography and Moiré Technique

All the dynamic impact tests reported in this work have been taken using one or two 16 mm

high speed framing cameras with a framing rate up to 22,000 frames per second (the image format on 16 mm film is 10 x 4 mm). Two methods of photography were adopted. One is regular high speed photography (no moiré) which included back surfaces and side view photography. The second method is high speed photography coupled with surface moiré fringes. The regular photography experiments were conducted using four 1000 watt photoflood lamps. The light intensity was further increased by pulsing the lamps to 2500 watts each during the impact event. The surface of the specimen was painted white to reflect more light.

The moiré fringe method is an optical phenomenon based on mechanical interference of light formed between two gratings: the one being the master grating (undeformed), while the other is the specimen grating (deformed). As the specimen grating is deformed, a fringe pattern is seen by the observer. Two different moiré methods to detect deflection were used. The first, which is commonly called the shadow-moiré, is achieved by painting the specimen with a reflective matte paint and illuminating it with collimated light. A grating placed close to the specimen face forms its shadow on the matte surface. The interference between the master grating and its (deformed) shadow results in a fringe pattern related to the out-of-plane displacement. The second method differs from the first by the fact that now the surface is mirrored and is illuminated by a diffused light source.

The matte reflective surface required for the shadow moiré was achieved by using a suitable undercoating. A mirrored surface was produced on the composite specimens by using a reflective tape (0.025 mm thick). The reflectivity of this surface was 75%.

To obtain the required amount of light from the shadow moiré, a 200 watt (4A, 50V, 10,000 lumnes) mercury lamp was employed. The amount of light was further increased by pulsing the lamp to 800 watts (40,000 lumnes) during the impact events.

A good quality fringe pattern depends on the type of grating used. A Runchi-ruling grid type was chosen for most of the experiments. Since the grids are destroyed during the tests, a replica of the Runchi ruling was formed by contact printing the ruling against high contrast photographic plate (2,000 lines per mm resolution). Another grating, especially to be used with the large specimen was constructed. This grid is formed by stretching thin Nylon line between two threaded (0.3 mm pitch) rods. This type of grid eliminates multiple reflection effects and results in better fringe quality than the other two grids. A 3 lines per mm grid was successfully obtained, which will be referred to as the wire grid. A photograph of this grid is shown in fig. 3.

e) Experimental Set-up

Two experimental set-ups were used during the impact test. One is mounted on a surface plate and a portable hydraulic press is used to apply the load. This set-up is shown in fig. 4. The large specimen required more load and a set-up was developed using a large hydraulic testing machine. This set-up is shown in fig. 5.

III. IMPACT EXPERIMENT RESULTS

A total of 17 graphite-epoxy laminates were impacted at the center by a 1.27 cm (0.5 in.) diameter aluminum sphere. The panel geometry, support and test conditions are given in Table II. For convenience the data are shown in fig. 6 along with the catastrophic strength threshold curve of ref. 1. As can be seen, the majority of the tests were carried out over a narrow range of velocity. This range was selected in the middle of what appears to be a transition in the threshold curve. The selection was made in the belief that more could be learned about the initial damage and subsequent damage propagation by tests in the transition region. The test points are somewhat lower than the threshold curve of ref. 1. However, that curve was drawn with limited data in the transition range.

The first tests were conducted using reflected light photography. Test panel A-2 is shown in fig. 7. The time between frames is 110 μs. Frame one of this sequence shows what appears to be a bulge in the surface. Extensive damage in the region near the edge is evident in the next frames.

Moiré high speed photography was used in subsequent tests. The parameters of the photographic set-up are given in Table III. The moiré fringes represent contours of equal displacement normal to the plate surface. The displacement for each fringe order varied from 0.14 mm to 0.34 mm (Table III).

The results for panel B-2 are shown in fig. 8. The impact point is not centered in the picture. The field of

view is 86 x 29 mm and the time between frames is 61 μs. The impact causes a peak displacement on the back surface of the order of 1 mm. This displacement changes very little for six frames (≈360 μs) indicating that it represents permanent deformation. Frame 8 shows a rapid growth which is interpreted to be bulging of the outer laminates of the panel. The growth appears to start at a slight angle to the horizontal. This pattern of growth was observed in some but not all subsequent tests. The most distinguishing feature of this sequence of photographs is the delay between the initial damage phase and the subsequent damage propagation phase. This feature will be discussed further in this report.

The results for test panels B-6 and B-9 are shown in figs. 9 and 10. These photographs show larger fields of view than that for B-2. The sequence of events is much the same as before but the time delay is different. B-6 (fig. 9) shows a delay of less than 50 μs (the time between frames) while B-9 exhibits a slow growth for about 200 μs, followed by a large deformation of the back surface.

Figure 11 shows the moiré photographs for test panel C-2. This panel is larger than those previously discussed (254 x 152 mm vs. 203 x 101 mm). The fringe quality is not particularly good for this series of photographs but the sequence of events can be detected. The rapid growth of the damage area does not begin until frame 24 (1200 μs). Prior to this the damage area is almost stationary with a slow

growth beginning in frame 17. Superimposed on this "permanent" deformation is what appears to be a plate vibration motion. The half period (ending in frame 16) corresponds to a frequency of about 600 Hz.

A photo sequence of an unloaded test panel (B-5) is shown in fig. 12. The maximum surface displacement observed was about 0.25 mm. No permanent deformation was observed from the moiré photograph.

The photographs for test panel B-4 are shown in fig. 13. The irregular dark pattern in this series of photographs is due to an optical interference. This panel was impacted at the same velocity as B-5 but was preloaded to a strain of 3180 μm/m. Catastrophic failure did not occur until approximately one minute after impact. The back surface permanent deformation was about 0.8 mm out of a total deformation of about 1.3 mm. Comparing this result to that of B-5 indicates some coupling of the in-plane load and the impact.

Several test panels were impacted and the side of the specimen photographed. These results are shown in fig. 14 for test panel A-3. The test panel is unsupported over the field of view shown in the film sequence. Frame 0 shows the projectile advancing towards the specimen. Impact was estimated to occur 45 μs after frame 0. Frame 2 shows a central crack extending the whole width of the photograph (85 μs after impact). The plate edge moves approximately 0.25 mm in frame 3. Additional cracks (delaminations) occur

in subsequent frames accompanied by front and rear surface buckling and complete rupture of the panel. This sequence of photographs (highlighted by the early appearance of an edge crack) led to similar tests on two other panels (AB-1, AB-3).

Tests AB-1 and AB-3 were photographed using two high speed cameras. One was used to record specimen back face (shadow moiré), while the other recorded the specimen side. Correlation between the two motion pictures thus obtained was achieved by using a common timing pulse (1 kHz) displayed on the developed film.

Test specimen AB-1 was supported with the small specimen support. A window along the side of the support was cut so that a side view photograph could be made. The panel was supported along its entire length. The moiré pattern obtained for test AB-1 is shown in fig. 15a and the side view is shown in fig. 15b (corresponding to the left side of fig. 15a). Based on the common timing pulse, it was found that frame 0' (side view) is 14 μs later than frame 0. The characteristic deformation propagated along the specimen width and reached the left side boundary in frame 6. Note that its tip is pointed down about 7 mm. Frame 6' (14 μs later than 6) shows an initial appearance of a central crack. In frame 7' the crack has extended through the full length of the pictures. This was accompanied by the appearance of a larger crack (5 mm long) pointed downward from the impact level (central

spot). The short crack appearance is attributed to the deformation recorded in frame 6. Frames 29' to 31' show the complete failure of the test specimen.

Test panel AB-3 was trimmed to its size from a large specimen type of lot number 2. The photographic results are given in figs. 16a and 16b. Frame 0' was calculated to be 30 μs before impact and 28 μs after frame 0. This test panel did not fail catastrophically and there is no evidence of any edge cracks. A permanent surface displacement of the order of 0.6 mm is visible in fig. 16a. The impact duration and rebound velocity were found to be 70 μs and 7 m/sec from fig. 16b.

The contours of surface displacements can be converted to displacements and displayed as displacement versus distance plots. This type of result is shown in fig. 17 for test panel B-9. The time between frames is approximately 50 μs. The rapid spreading of the damage is evident after frame 4. The velocity of this spreading will be discussed in the next section.

IV. DISCUSSION AND CONCLUSION

In this section the progression of failure is interpreted based on the appearance of the photographic moiré records. In order to accomplish this interpretation it is important to recognize or show that the moiré patterns actually observed can be directly related to the damage which the plate has incurred.

When a plate is impacted by a projectile two gross phenomena are likely to occur. First, the plate is set into vibration. Second, damage may be inflicted upon the plate. It is of primary interest to follow the damage in the plate. Since the recording method is based on moiré fringes, however, total displacements are measured. Thus both displacements, those associated with the incurred damage as well as those resulting from the vibration of the plate are measured. The question therefore arises as to whether the two phenomena can be separated reasonably well. It is believed that this is possible in view of fig. 16. It is evident in this picture sequence that in every fourth exposure approximately the same fringe pattern appears. Since there is a time step of close to 50 μs between each frame the picture sequence indicates that the plate vibrated with a period of about 400 μs. Note also that the peak amplitude of approximately 1 fringe corresponds to a displacement of 0.33 mm.

It is also clear from this sequence of photographs that the displacement peak under the impact point stands out rather distinctly from the general background of the plate vibration.

It appears, therefore, that the displacement peak under the impact point at early times exceeds the general vibrational deformations of the plate by a good margin, namely by a factor of approximately 3.

The latter displacement peak appears to represent permanent damage of the plate. If the projectile velocity exceeds a velocity on the order of 65 m/sec, this displacement peak appears on the side opposite from the impact point. The displacement peak does not disappear with time which indicates that irreversible deformation has occurred within the plate in that vicinity. This phenomenon is clearly evidenced in test panels AB-3 (fig. 16) and B-4 (fig. 13). In these instances the impact was not sufficiently energetic to carry the plate to complete destruction through delamination and subsequent buckling failure. However, permanent residual deformation is clearly evidenced superposed on the vibratory motion of the plate as a background.

The next stage in the failure scenario is the spreading of the damage region. Back surface moiré photographs show a rapidly expanding area of deformation. Connecting this deformation to a spreading damage area is easy to visualize but harder to quantify in detail.

It has been noted in one particular experiment that cracks could be observed to appear along the edge of the specimen. As a consequence, two cameras were set up to simultaneously record moiré fringes on the backside of the specimen plate and

to observe its edge. It is clear by looking at the edgewise photograph of the plate (fig. 15b) that the first crack appears at the edge at roughly the time at which in the other picture (fig. 15a) the moiré pattern has reached the left boundary of the plate. As a result of this experiment the front of the internal propagating delamination has been associated with the first or lowest order fringe in the moiré pattern. This assignment of the propagation front is a bit arbitrary; however, for the present purposes of an engineering interpretation of the phenomenon occurring in the damage progression it seemed quite sufficient. Further examination of the propagating damage will use this definition for the extent of the damage region.

Another observation of interest has to do with the time at which the damage spreads after initial impact has occurred. In this connection it is well to remember that most of the experiments were conducted in the vicinity of projectile velocity of 60-70 m/sec. According to fig. 6, this falls into the steeper portion of the curve relating failure strain to projectile velocity. For most of the experiments it was quite clear that damage in the form of a displacement peak under the impact point occurred very rapidly but the damage did not spread immediately. For example, in fig. 11 it took something like 24 frames or the equivalent of 1.2 ms before the damage started to grow significantly. After it started to grow, the growth was relatively rapid. Again, by comparison fig. 8 shows that damage did not appear to grow for

approximately eight frames or the equivalent of 0.5 ms and then grew very rapidly. Finally, from fig. 9 it is evident that damage grew almost from the very beginning of impact. While it may on cursory examination appear that there may be two modes under which damage spreads it is believed that this is related to the strain level. Panels that are closer to the threshold curve tend to have an early propagation of the damage area while those further away exhibit a slight delay of propagation.

It is of interest to ask whether the propagation behavior is significantly different depending on whether the damage spreads early or late in the impact history. The experiments indicate that the spreading phenomenon is either insensitive to, or hardly affected by, the time at which early propagation occurs. To illustrate that point refer to fig. 18, where the location of the first fringe is shown as a function of time, producing an x-t diagram. This is done for six different tests. While the number of data points are not large enough to give conclusive evidence it seems rather clear that the propagation velocity as indicated by the slope of the curves tends to be rather much the same from one shot to the next. Curve number B-6 corresponds to a delamination that started to propagate almost immediately, while curve AB-1 corresponds to one which seems to have propagated, arrested somewhat, then propagated further. Curve B-9 corresponds to a plate experiment in which the delamination propagated slowly at first but eventually

propagated with approximately the same speed as that which occurred for curve B-6. Finally, the delamination corresponding to test B-2 indicates that no propagation occurred for about seven frames and after that when it did occur it again propagated at approximately the same rate as curves B-7 and B-9. The curves on the left hand part of the figure simply refer to the left most point in the moiré diagram and similar statements hold with regard to these curves. These observations are important because they support the intuitive feeling that the propagation problem is separate from the problem of damage generation. If this statement can be further supported and accepted it would basically make it possible to treat the damage propagation problem separate from the impact problem, which has great analytical advantages.

Having commented on the time history of the delamination spreading, it is of interest to indicate an estimate of the rate at which this spreading occurs. This information can be directly found using fig. 18. From this figure it was deduced that the maximum velocity falls in the range of 1.4×10^3 m/sec to 3.3×10^3 m/sec. The average value of this maximum was 1.9×10^3 m/sec (7500 in/sec). While this velocity is substantial it is slow compared to a typical in-plane wave velocity for this material.

A further phenomenon which is clearly repeatable deals with the geometry of the subsequent spreading of the damage and the way in which the final failure of the plate is

approached. In viewing figs. 8 through 10, it is clear that the initial deformation resulting from impact damage is nearly circular in shape, but invariably when spreading occurs, it does so in a transverse direction, that is, horizontally. Bearing in mind that in all these figures the load is applied along an axis from top to bottom of the figure, it shows clearly that the delamination occurs at right angles to the compressive load. It is believed that the reason for this phenomenon is based on fracture mechanics and energetic considerations. The damage area is somewhat like a section of reduced modulus. Local buckling of the delaminated region shifts the stress distribution in a manner similar to that resulting from a hole. The high stress regions are on a line normal to the load axis. Some spread parallel to the load axis is evident but the predominant propagation is normal to the load axis.

Having tentatively established so far when and how rapidly the delamination propagates it is appropriate to comment on the final stages of the compression failure. In fig. 15b, the edge view of a specimen is recorded. The point where a single central crack has appeared and further damage results in a gross fashion occurs in the frames after and including frame 29'. The time corresponding to frame 30' is about 1.5 ms after impact. There are two reasons why this final failure phenomenon may occur at this time. First, since the natural frequency of vibration is on the order of 2000 Hz, the phenomenon might possibly be related

to the vibration of the plate. However, one might expect that the maximum stress occurs during the early part of the plate vibration, namely the quarter period, so that the phenomenon should have occurred at something like 0.1 or 0.2 ms. This clearly did not occur. The second phenomenon that may have caused this occurrence at this time may be the dynamics of the testing machine. It is quite reasonable to expect for testing machines of this size* to have time responses in the millisecond range. For this reason it is assumed that the occurrence of the total damage phenomenon at this time is related to the time it takes for the testing machine to adjust to the damage and more compliant compression specimen.

To summarize the observations to date then, it can be stated that irreversible damage is relatively easy to discern because it is associated with irreversible displacements. The early stages of crack or delamination propagation is a phenomenon subject to sizeable statistical scatter. When spreading of the delamination occurs it does so relatively consistently with a velocity of approximately 200 m/sec in the range of strains and impact velocities explored. Spreading of the damage occurs primarily at right angles to compression load.

---

*A large hydraulic testing machine, 1335 kN capacity.

REFERENCES

1. Rhodes, M.D., Williams, J.G., and Starnes, J.H. Jr., "Low-Velocity Impact Damage in Graphite-Fiber Reinforced Epoxy Laminates," Presented at the 34th Annual Conference Reinforced Plastics/Composite Institute, New Orleans, LA, Jan. 29 - Feb. 2, 1979.

2. Rhodes, M.D., Williams, J.G., and Starnes, J.H. Jr., "Effect of Impact Damage on the Compression Strength of Filamentary-Composite Hat-Stiffened Panels," Presented at the 23rd SAMPE National Symposium and Exhibition, Anaheim, CA, May 2-4, 1978, SAMPE Vol. 23, "Selective Application of Materials for Products & Energy," pp. 300-319, May 1978.

3. Rhodes, M.D., Williams, J.G., and Starnes, J.H. Jr., "Effect of Low-Velocity Impact Damage on the Compressive Strength of Graphite-Epoxy Hat-Stiffened Panels," NASA Technical Note D-8411, April 1977.

4. Starnes, J. H. Jr., Rhodes, M. D., and Williams, J. G., "The Effect of Impact Damage and Circular Holes on the Compressive Strength of a Graphite-Epoxy Laminate," NASA Technical Memorandum 78796, October 1978.

5. Williams, J.G., Anderson, M.S., Rhodes, M.D., Starnes, J.H. Jr., and Stroud, W.J., "Recent Developments in the Design, Testing and Impact-Damage Tolerance of Stiffened Composite Panels," NASA Technical Memorandum 80077, April 1979.

6. Mikulas, M.M. Jr., Bush, H.G., Rhodes, M.D., "Current Langley Research Center Studies on Buckling and Low Velocity Impact of Composite Panels," Third Conference on Fibrous Composites in Flight Vehicle Design, Part II, NASA TM X-3377, pp. 633-663, 1976.

Table I
Composite Panel Material Properties

Lay up $(\pm 45/0_2/\pm 45/0_2/\pm 45/0/90)_{2S}$

Longitudinal modulus, GN/m^2 (lbf/in^2)	131 (19.0×10^6)
Transverse modulus, GN/m^2 (lbf/in^2)	13.0 (1.89×10^6)
Shear modulus, GN/m^2 (lbf/in^2)	6.41 (0.93×10^6)
Major Poisson's ratio	0.38
Density, g/cm^3 (lbm/in^3)	1.52 (0.055)
Ply thickness, mm (in.)	0.14 (0.0055)

$$\begin{Bmatrix} N_y \\ N_y \\ N_{xy} \\ M_x \\ M_y \\ M_{xy} \end{Bmatrix} = \begin{bmatrix} A_{11} & A_{12} & A_{16} & & & 0 & & \\ A_{12} & A_{22} & A_{26} & & & & & \\ A_{16} & A_{26} & A_{66} & & & & & \\ & & & D_{11} & D_{12} & D_{16} & & \\ & 0 & & D_{12} & D_{22} & D_{26} & & \\ & & & D_{16} & D_{26} & D_{66} & & \end{bmatrix} \begin{Bmatrix} \varepsilon_x \\ \varepsilon_y \\ \gamma_{xy} \\ K_x \\ K_y \\ K_{xy} \end{Bmatrix}$$

$$\varepsilon_x = \frac{\partial u}{\partial x}\ ,\ \varepsilon_y = \frac{\partial v}{\partial y}\ ,\ \gamma_{xy} = \frac{\partial v}{\partial x} + \frac{\partial u}{\partial y}$$

$$K_x = -\frac{\partial^2 w}{\partial x^2}\ ,\ K_y = -\frac{\partial^2 w}{\partial y^2}\ ,\ K_{xy} = -2\frac{\partial^2 w}{\partial x \partial y}$$

Dimension: A = GN/m (lbf/in) , D = GN-m (lbf-in)

$A_{11} = .531$	(3.033×10^6)
$A_{22} = .263$	(1.505×10^6)
$A_{12} = .126$	(0.721×10^6)
$A_{66} = .136$	(0.774×10^6)
$A_{16} = A_{26} = 0$	
$D_{11} = 2.000 \times 10^{-6}$	(17.71×10^3)
$D_{22} = .890 \times 10^{-6}$	(7.88×10^3)
$D_{12} = .516 \times 10^{-6}$	(4.57×10^3)
$D_{66} = .551 \times 10^{-6}$	(4.88×10^3)
$D_{16} = .026 \times 10^{-6}$	(0.23×10^3)
$D_{26} = .026 \times 10^{-6}$	(0.23×10^3)

Table II
Test Panel Geometry, Support and Impact Conditions

Test Panel	Panel Size (mm)	Test Panel Holder	Impact Velocity (m/sec)	Pre Strain (μm/m)	Post Test Conditions	Lot Number
A-1	152 x 99 x 5.7	Small	61.0	3200*	Not failed	0
A-2	152 x 101.4 x 6.1	Small	63.3	3500*	Failed	1
A-3	152 x 99 x 6.1	Partially free sided	65.1	3458	"	1
B-1	203.2 x 101.4 x 6.1	Small	63.3	3335	"	1
B-2	185.4 x 101.4 x 6.1	"	"	3250	"	1
B-3	"	"	66.2	3220	"	1
B-4	203.2 x 101.4 x 6.1	"	65.1	3178	"**	1
B-5	"	"	"	190*	Not failed	1
B-6	"	"	"	3510	Failed	1
B-7	"	"	69.0	100*	Not failed	1
B-8	"	"	65.1	3273	"	1
B-9	"	"	"	3376	Failed	1
C-1	254 x 152.4 x 5.9	Large	69.0	3810	"	2
C-2	"	"	69.0	3690	"	2
AB-1	203.2 x 101.4 x 6.1	Small	76.0	2940	"	1
AB-2	"	"	29.0	8620	Not failed	1
AB-3	152 x 101.4 x 5.9	Partially free sided	65.1	3500	"	2

* Calculated from load measurement
** Specimen failed after ∿1 min.

Table III
Photographic Information

Test Panel	View	Field of View (mm)*	Frames/sec.	Fringe*** Constant (mm)
A-1	Back surface	Full field	9000	
A-2	"	Full field	9000	
A-3	Side	6.1 x 64	15500	
B-1	Back surface	25 x 25	20000	.19
B-2	"	85.7 x 29**	16500	.18
B-3	Front & back surface		19000 & 20000	.29 & .32
B-4	Back surface	96 x 78.4	21000	.33
B-5	"	96 x 86.4	20000	.27
B-6	"	96 x 75.4	20000	.29
B-7	"	96 x 115	20000	.14
B-8	"	96 x 54	19000	.29
B-9	"	95 x 84	19900	.30
C-1	"	141 x 103.5	19800	.34
C-2	"	141 x 98.5	19000	.32
AB-1	Back surface & side	86.4 x 68.6 & 6.1 x 45	19800 & 18150	.30
AB-2	"	"	20000 & 19000	.30
AB-3	"	86.3 x 70 & 6.1 x 43	18400 & 19800	.33

*First coordinate measures width and second measures length of the photographed area.
**Field is not centered around impact site.
***Fringe constant is the displacement difference between two adjacent fringes.

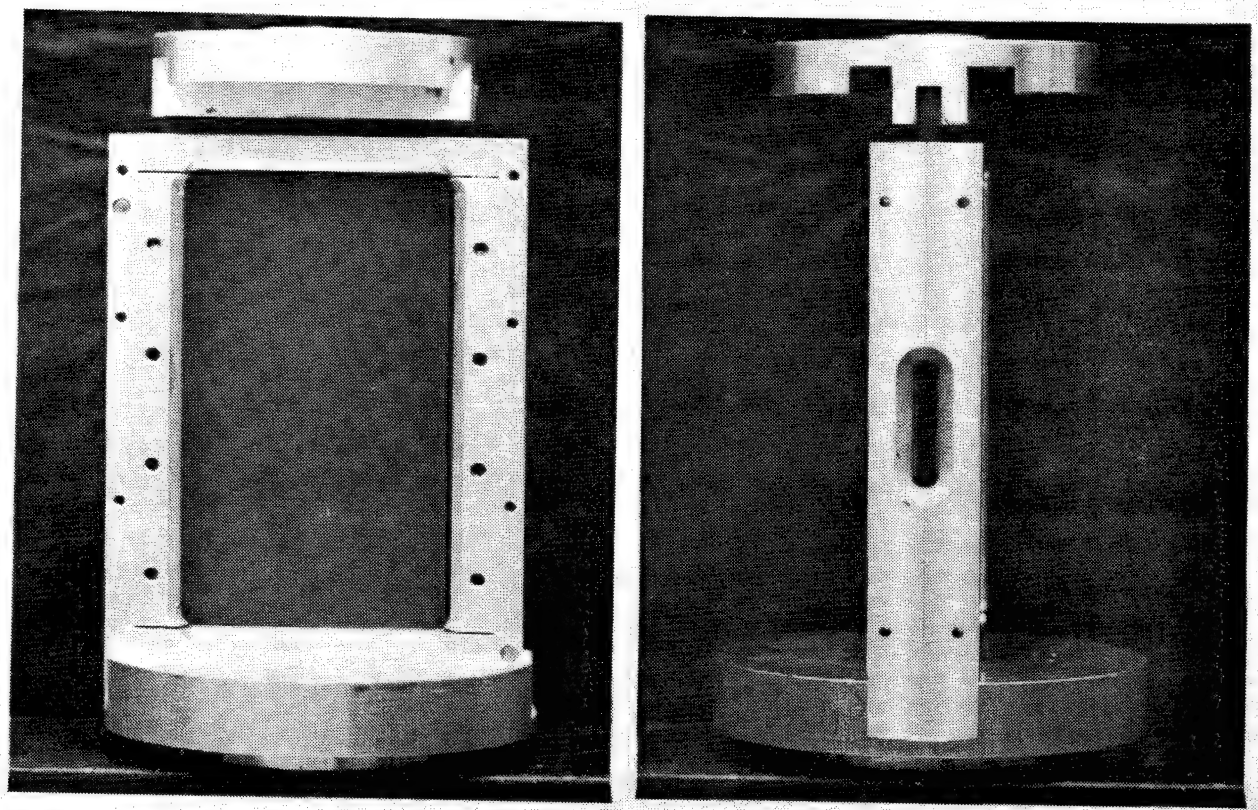

Fig. 1a Small Test Panel Support Fixture

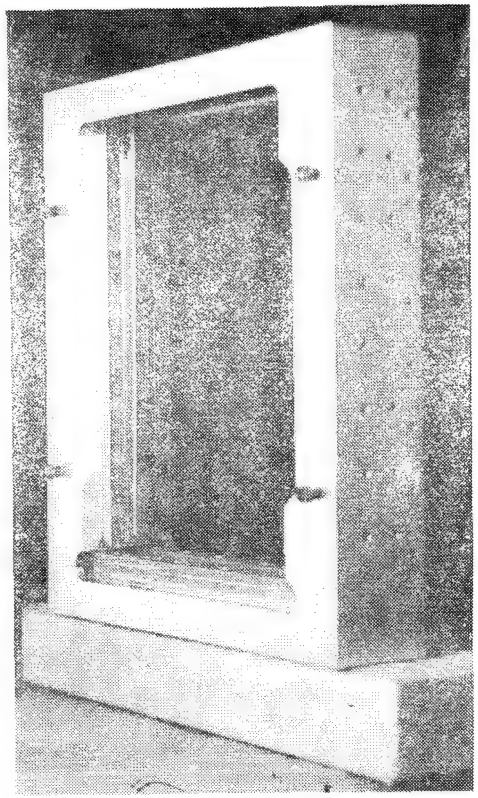

Fig. 1b Large Test Panel Support Fixture

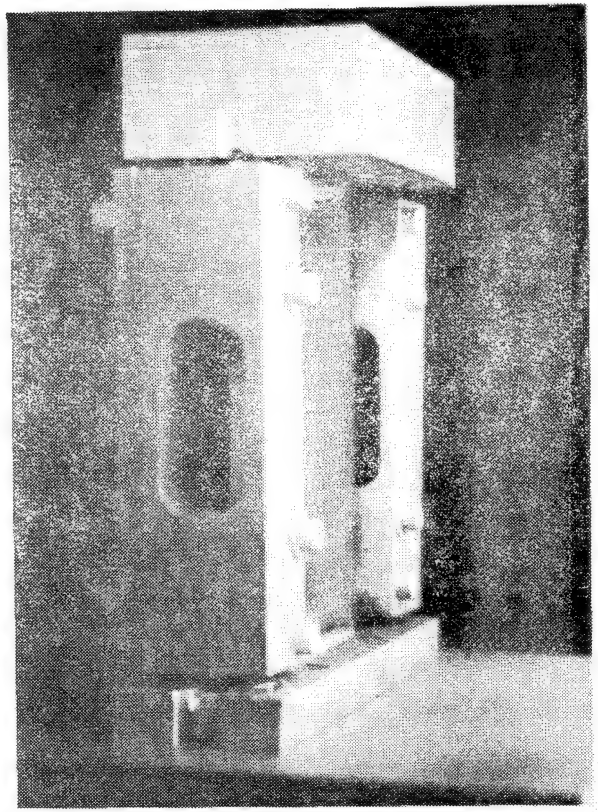

Fig. 1c Partially Free Sided Test Panel Support Fixture

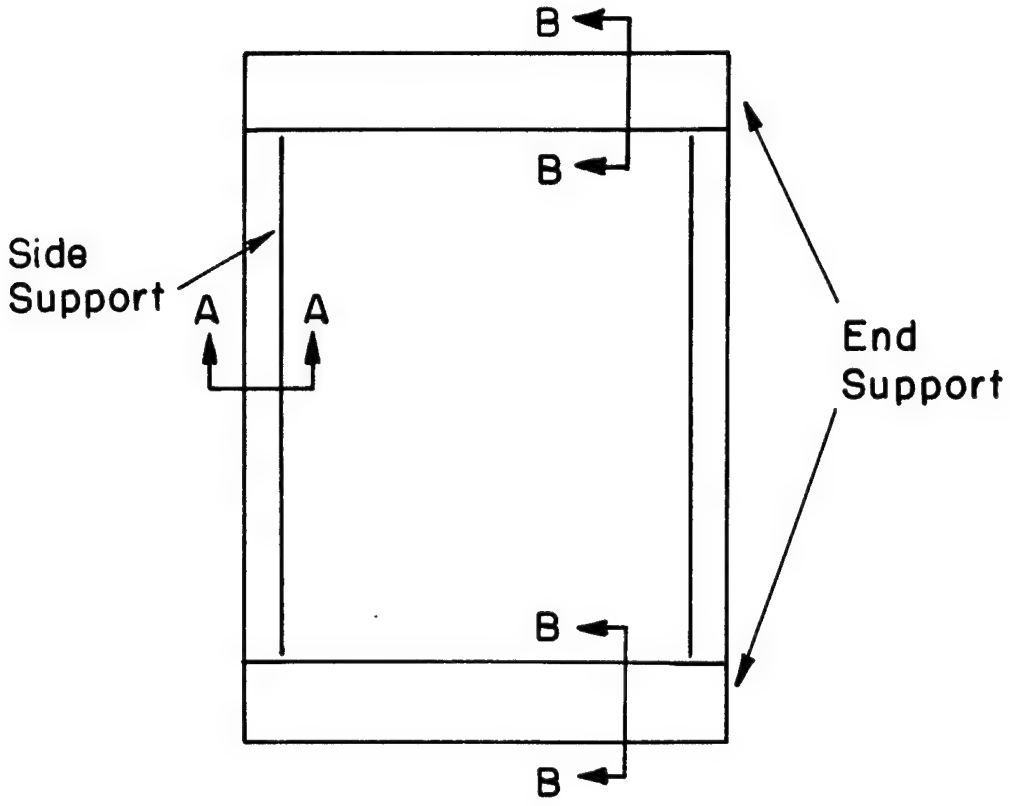

Section B - B

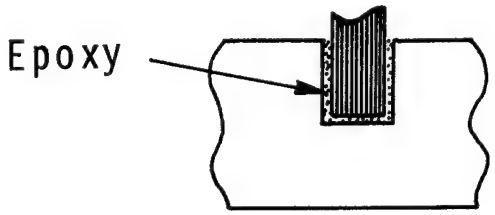

Section A - A

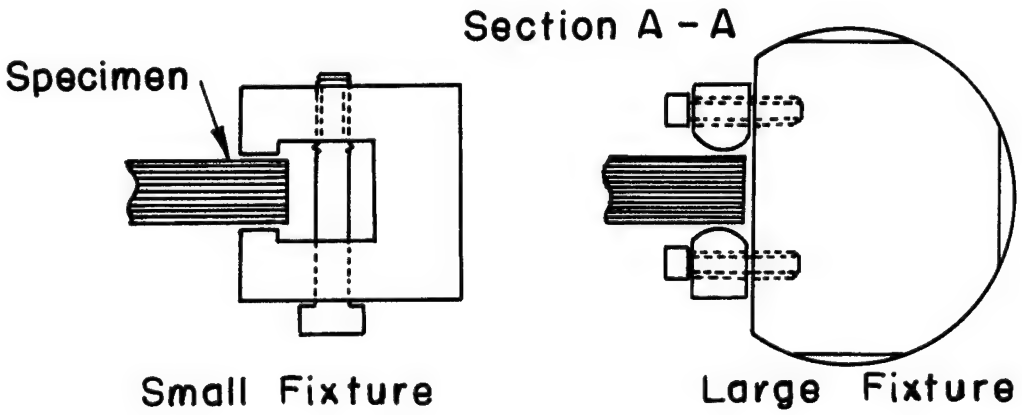

FIG. 2 TEST PANEL EDGE SUPPORTS

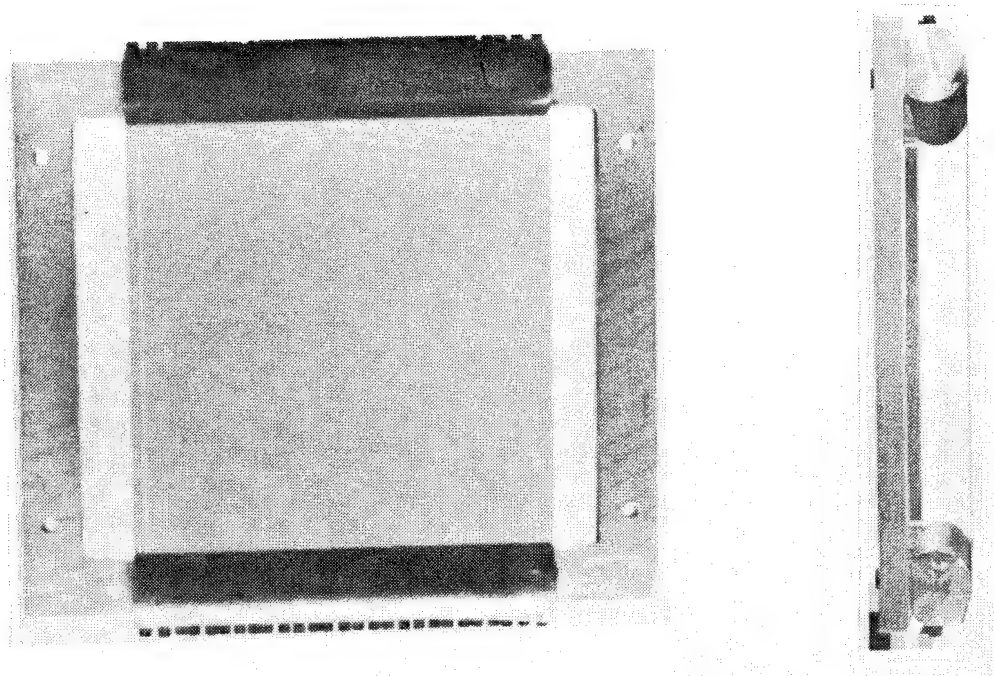

Front view

Side view

Fig. 3 The Wire Grid Used with Large Test Panel Fixture

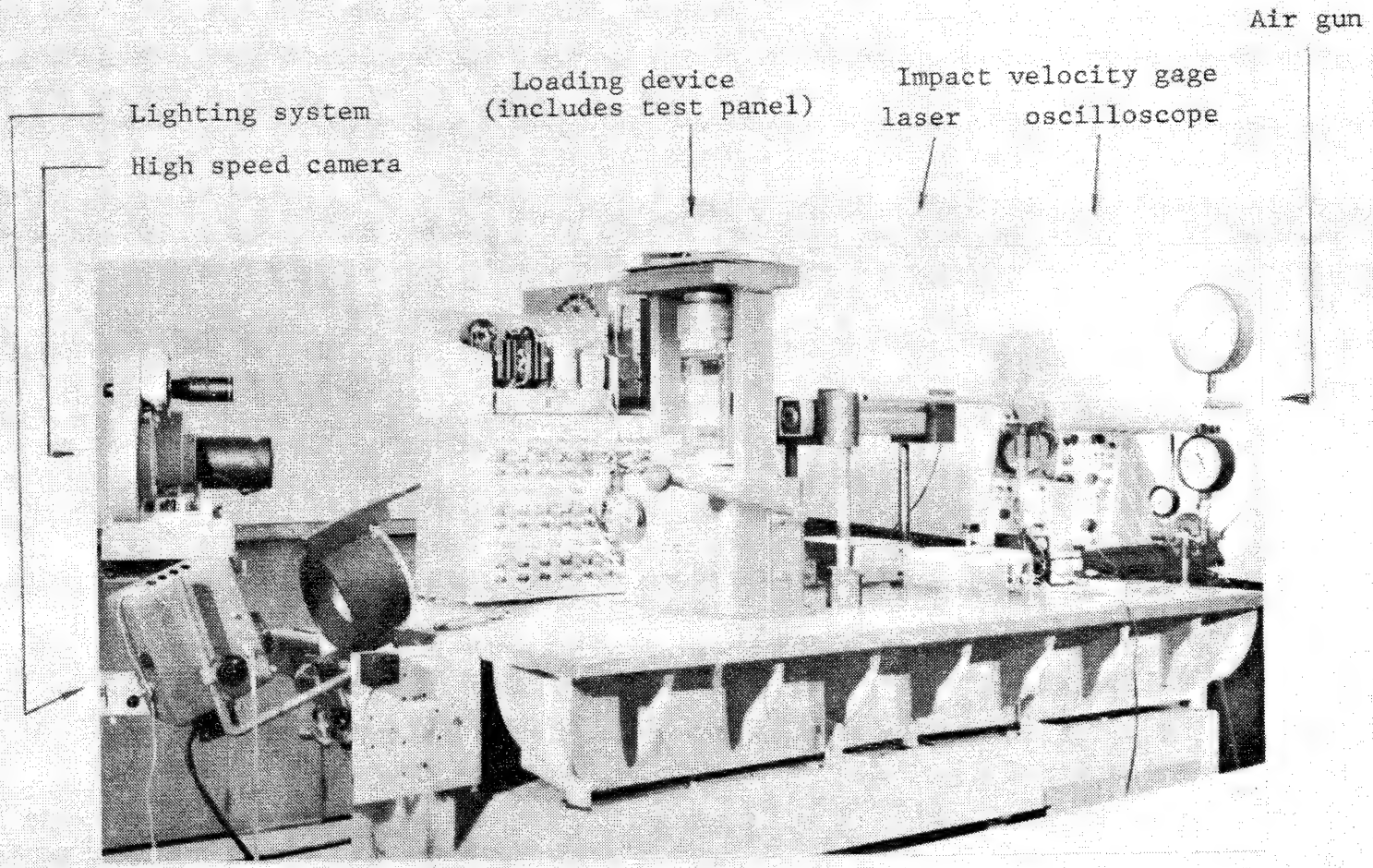

Fig. 4 Low Speed Impact Test Set-up Used with Small Test Panels

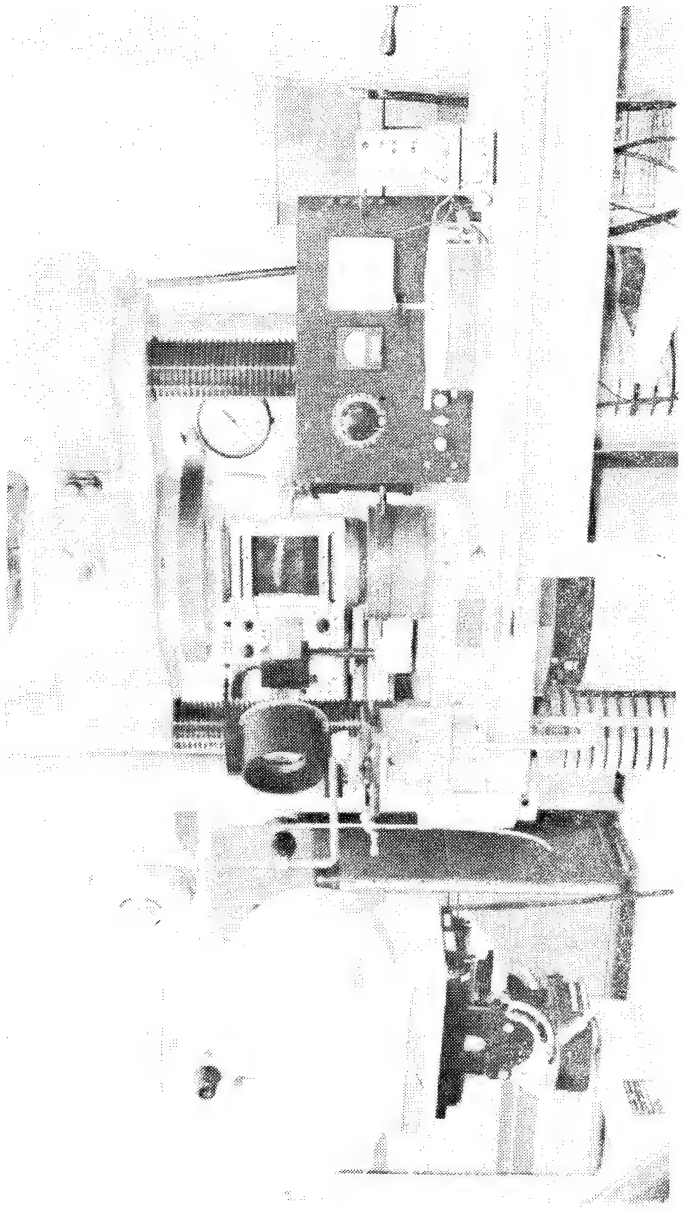

Fig. 5 Low Speed Impact Test Set-up Used with Large Test Panels

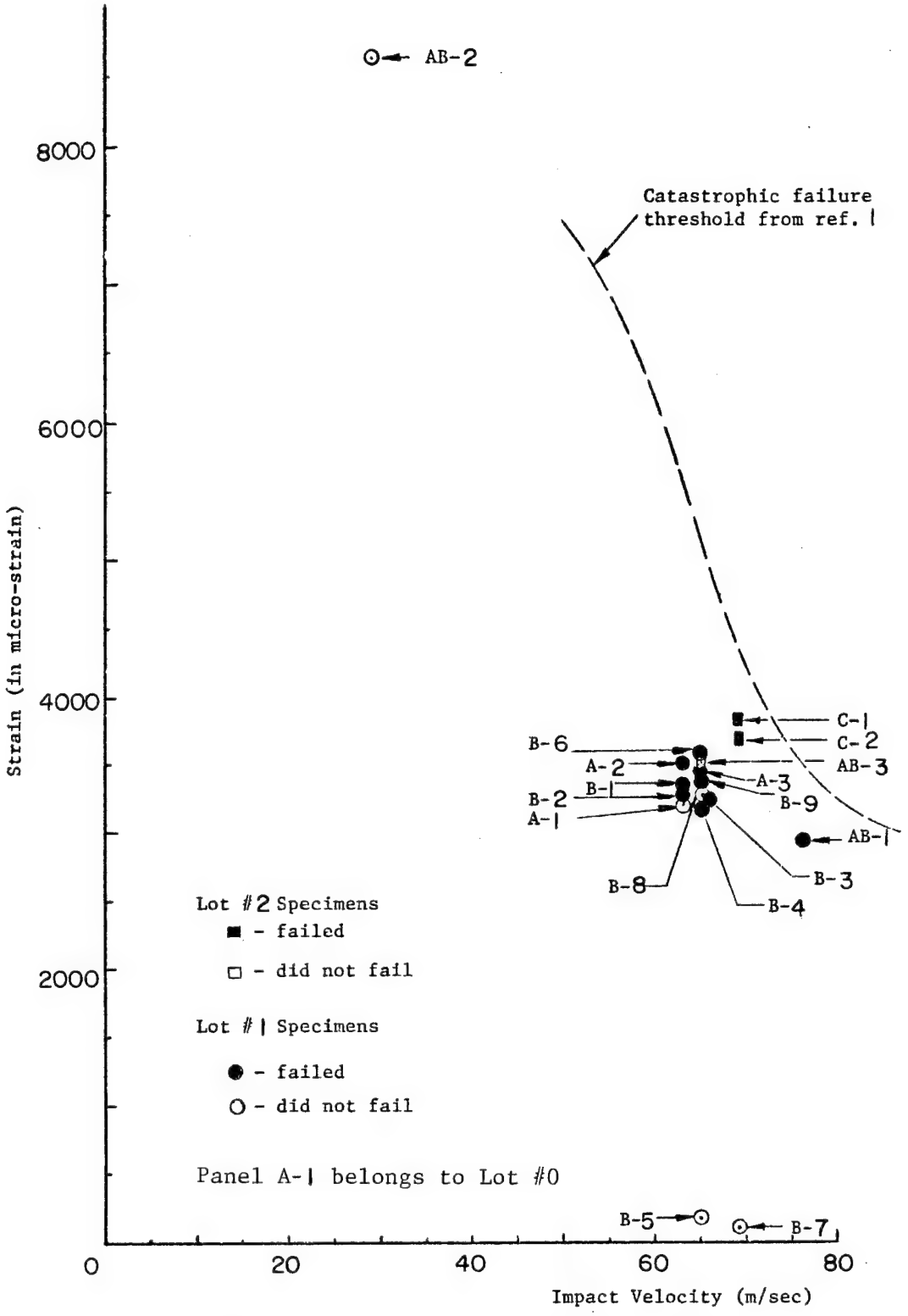

Fig. 6 Impact Experiment - Velocity vs. Strain

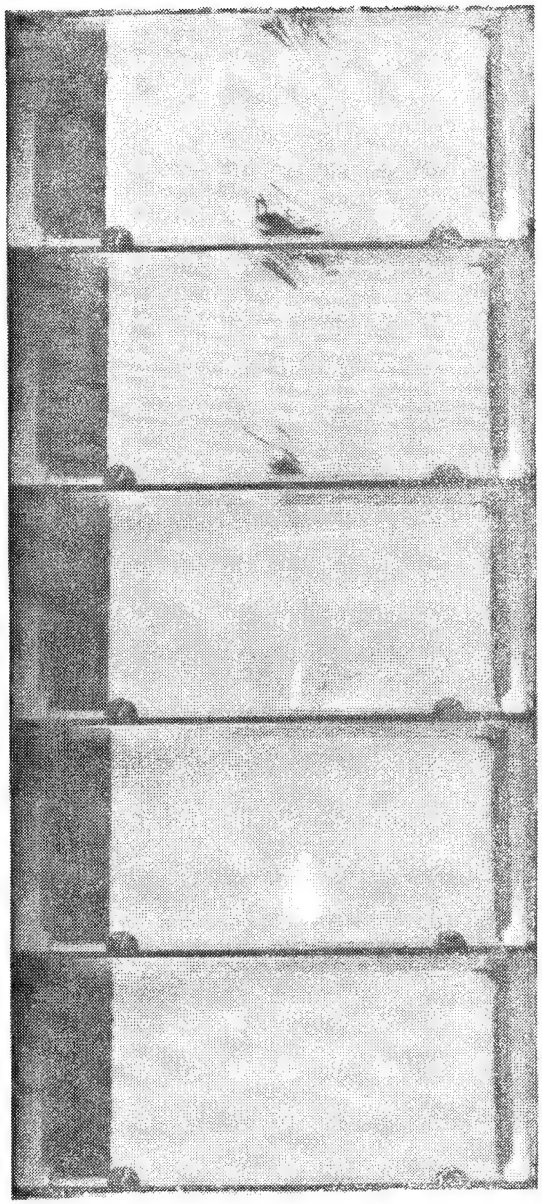

Fig. 7 Test Panel A-2, 9,000 frames/sec.

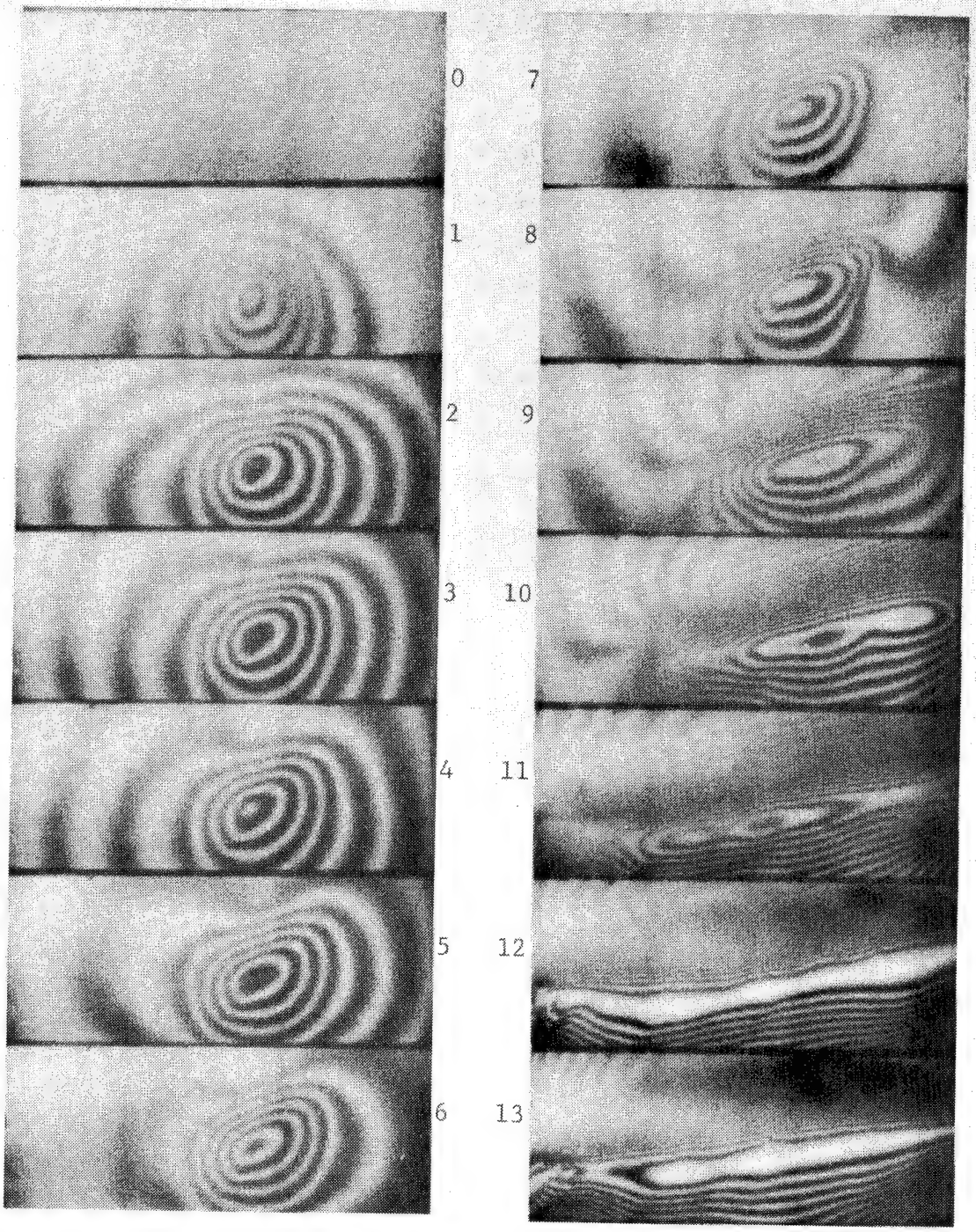

Fig. 8 Test Panel B-2, 16,500 frames/sec.

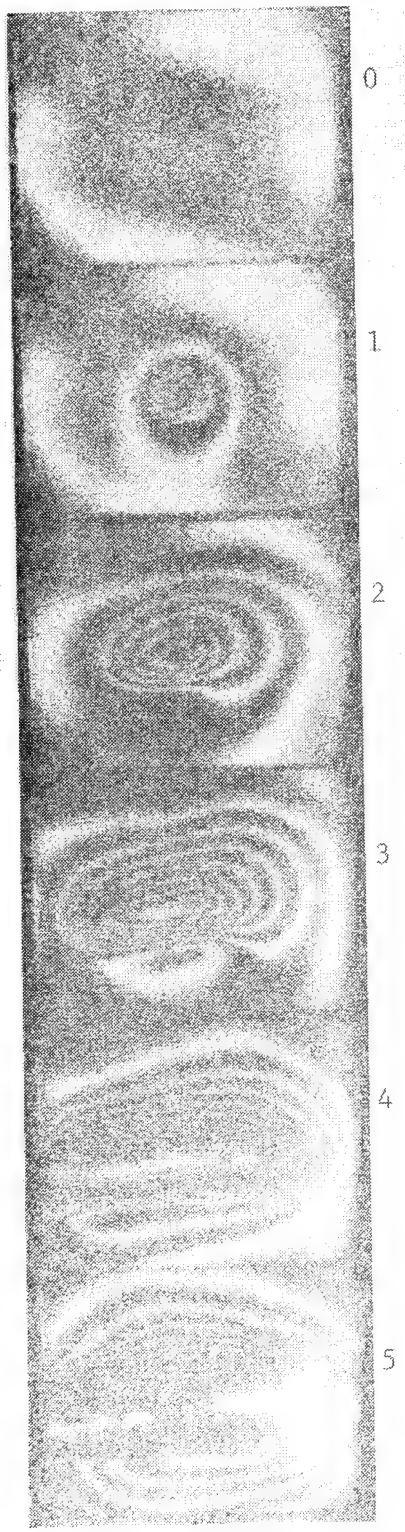

Fig. 9 Test Panel B-6, 20,000 frames/sec.

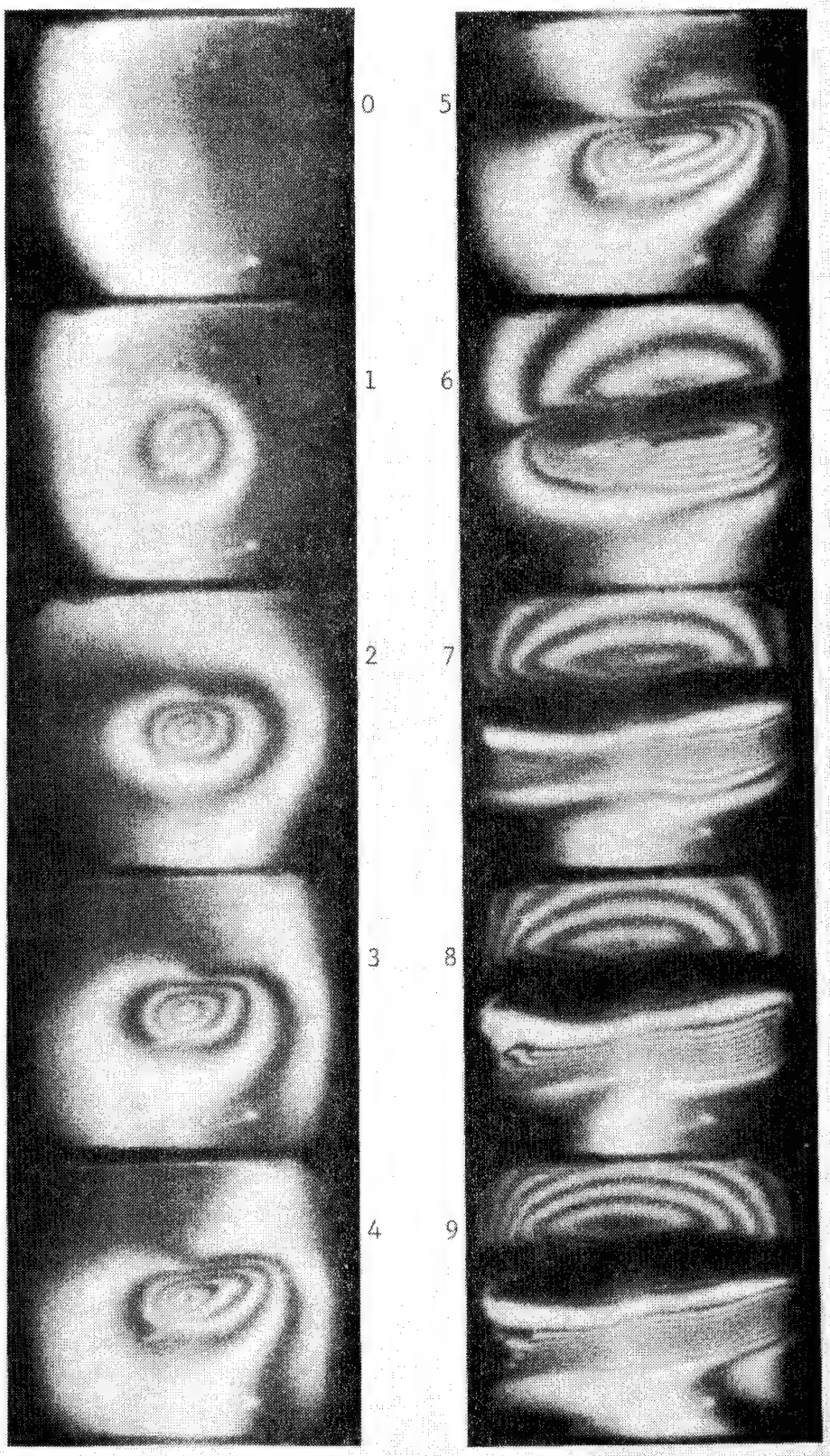

Fig. 10 Test Panel B-9, 19,900 frames/sec.

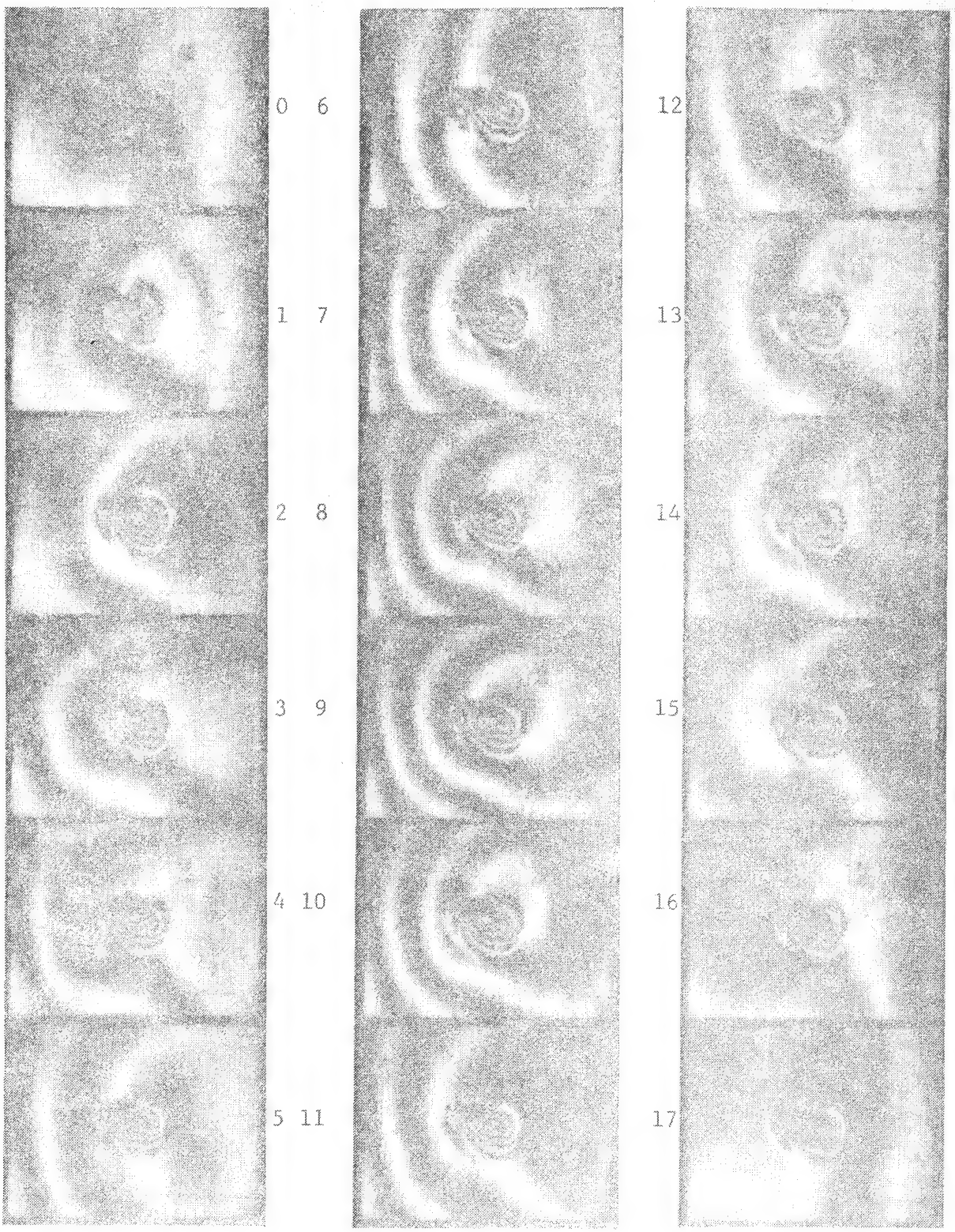

Fig. 11 Test Panel C-2, 19,000 frames/sec.

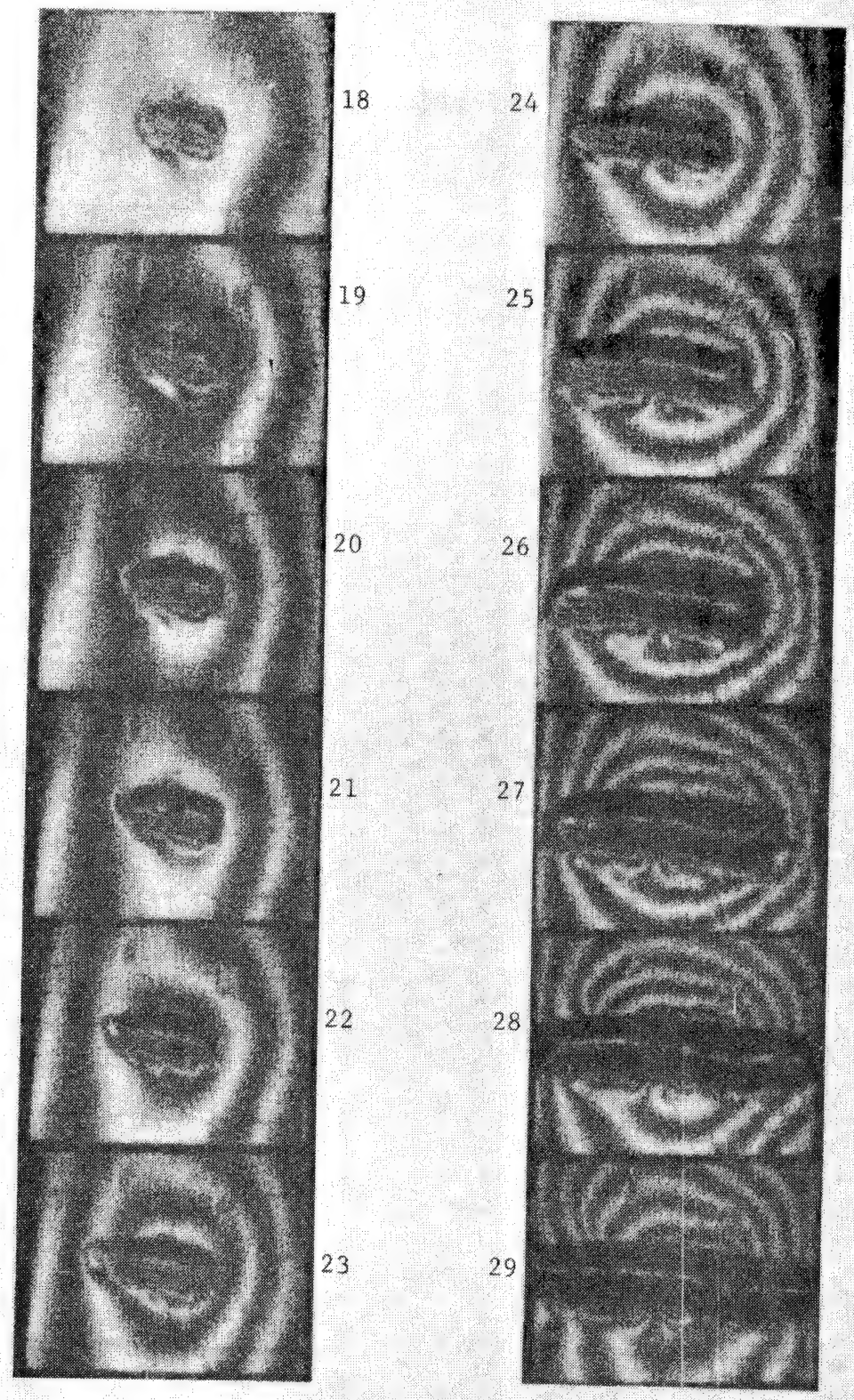

Fig. 11 Continued

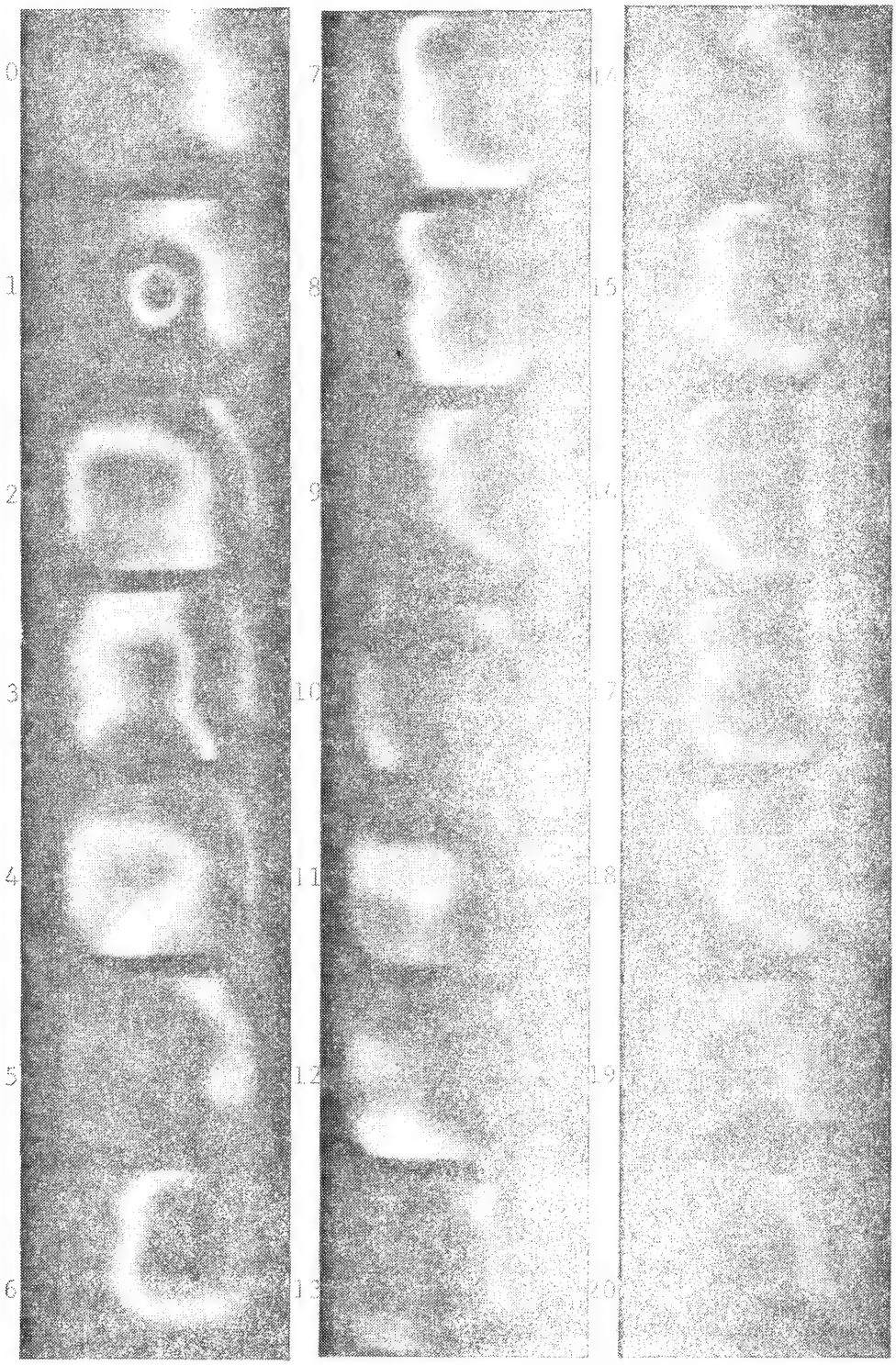

Fig. 12 Test Panel B-5, 20,000 frames/sec.

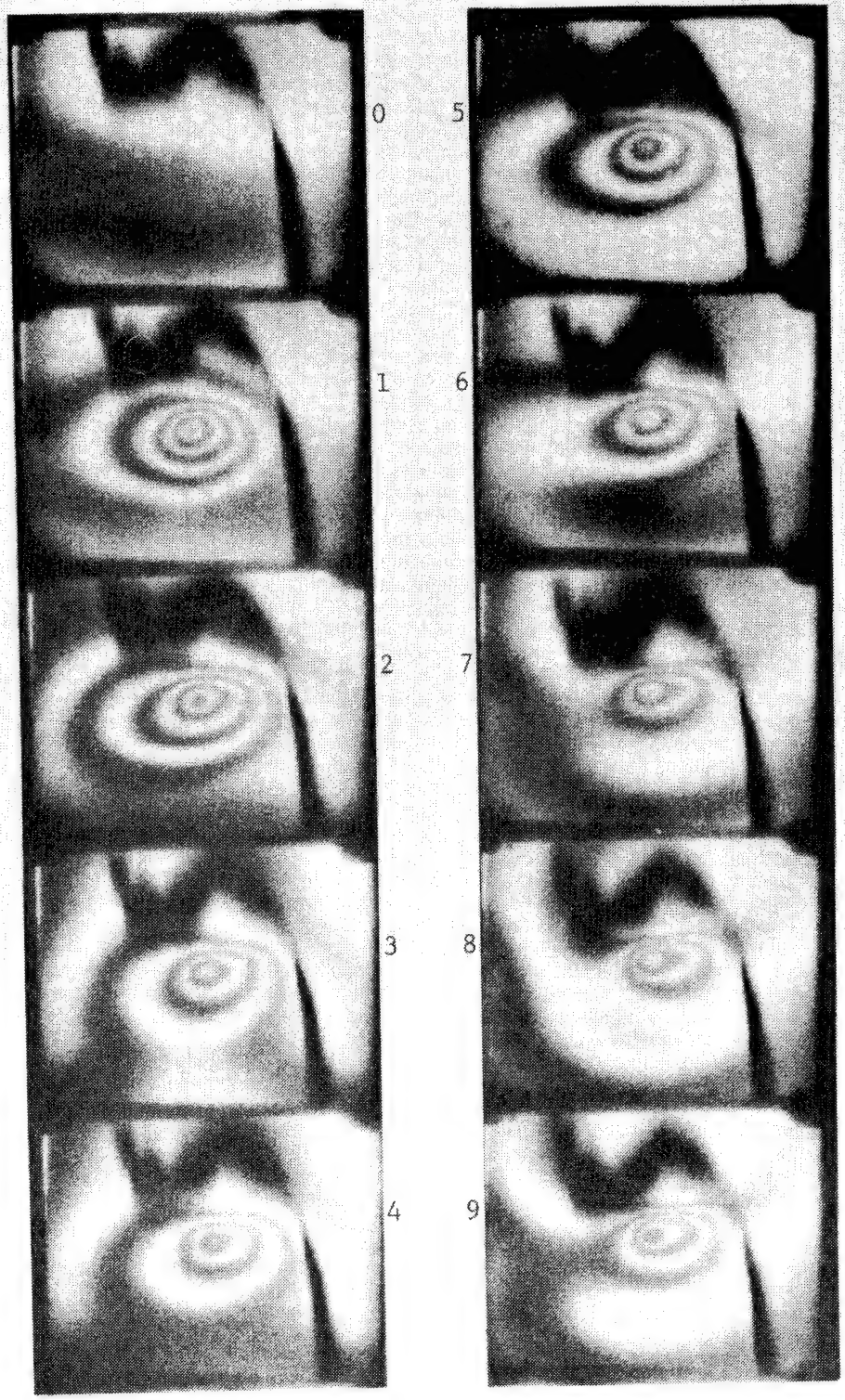

Fig. 13 Test Panel B-4, 21,000 frames/sec.

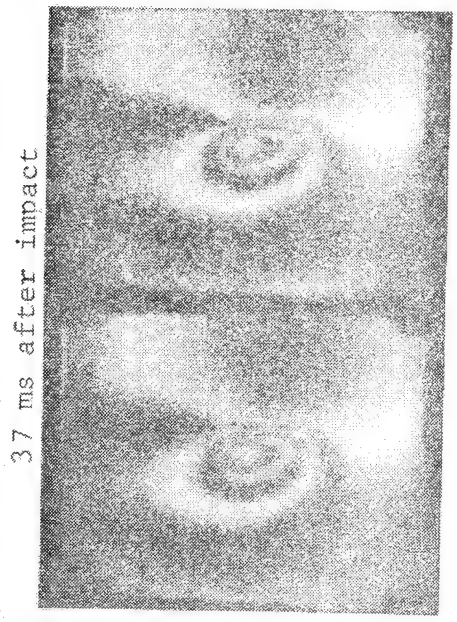

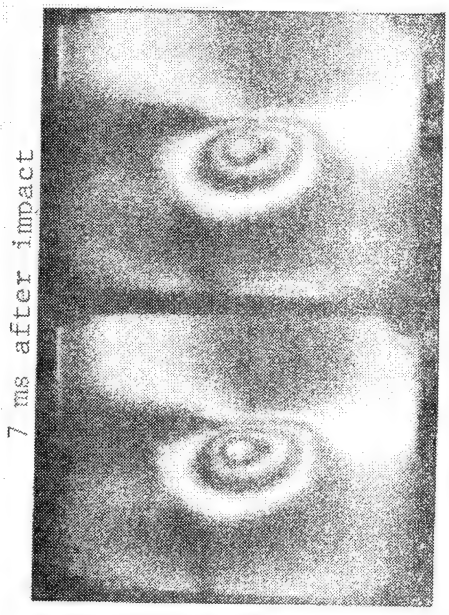

Fig. 13 Continued

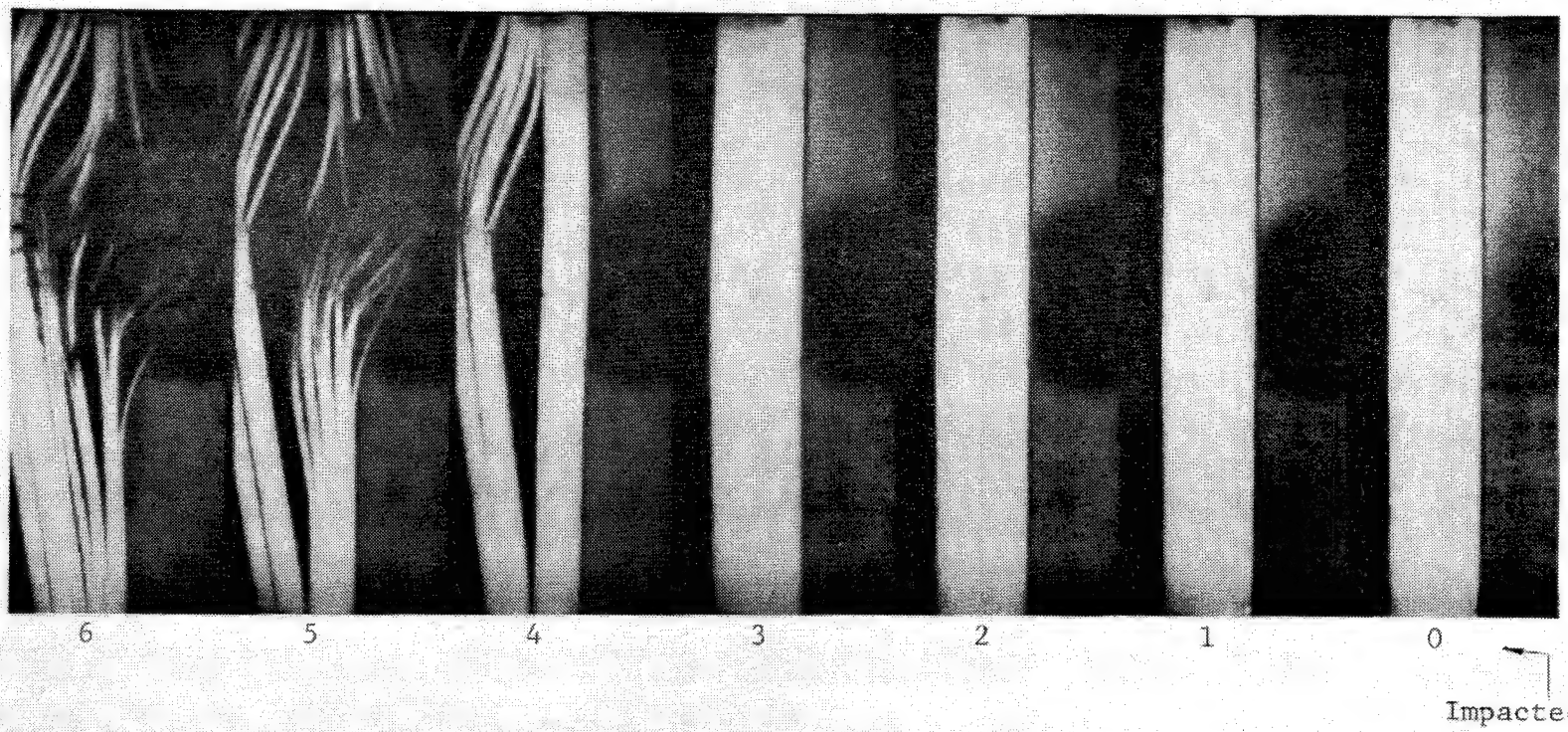

Fig. 14 Test Panel A-3, 15,500 frames/sec. (The portion of the test panel shown is free from support.)

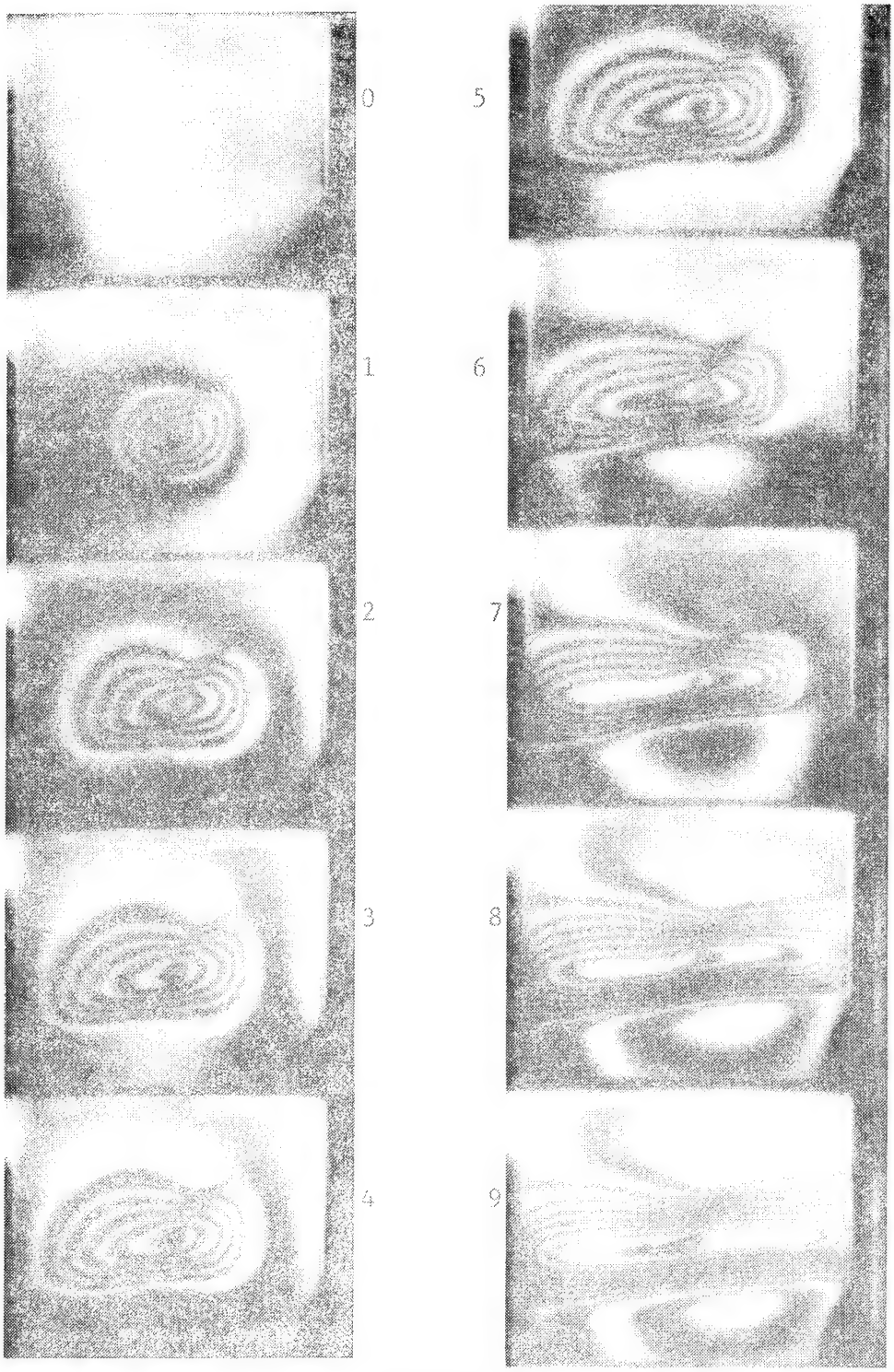

Fig. 15a Test Panel Ab-1, 19,800 frames/sec.

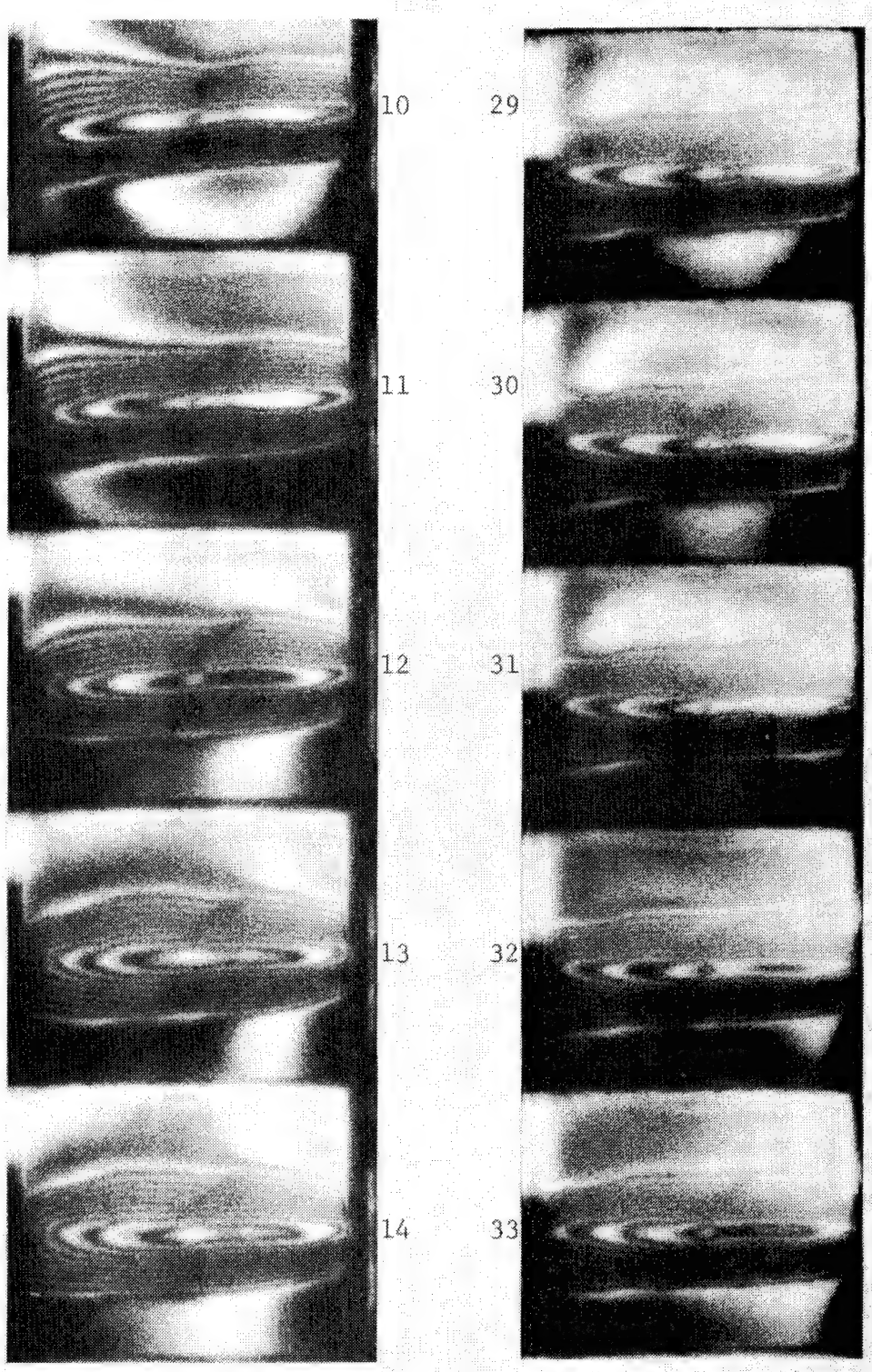

Fig. 15a Continued

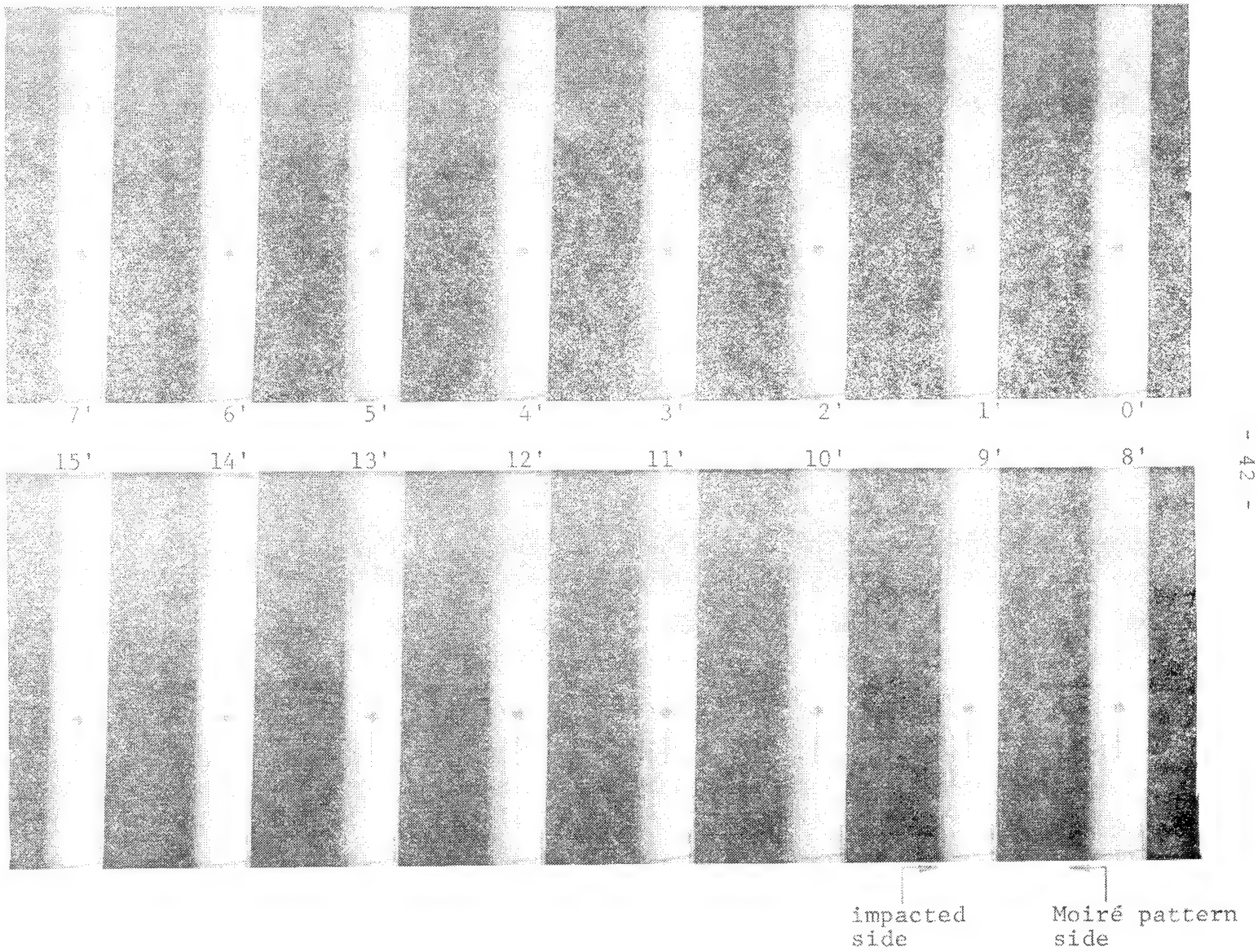

Fig. 15b Test Panel AB-1, 18,150 frames/sec.

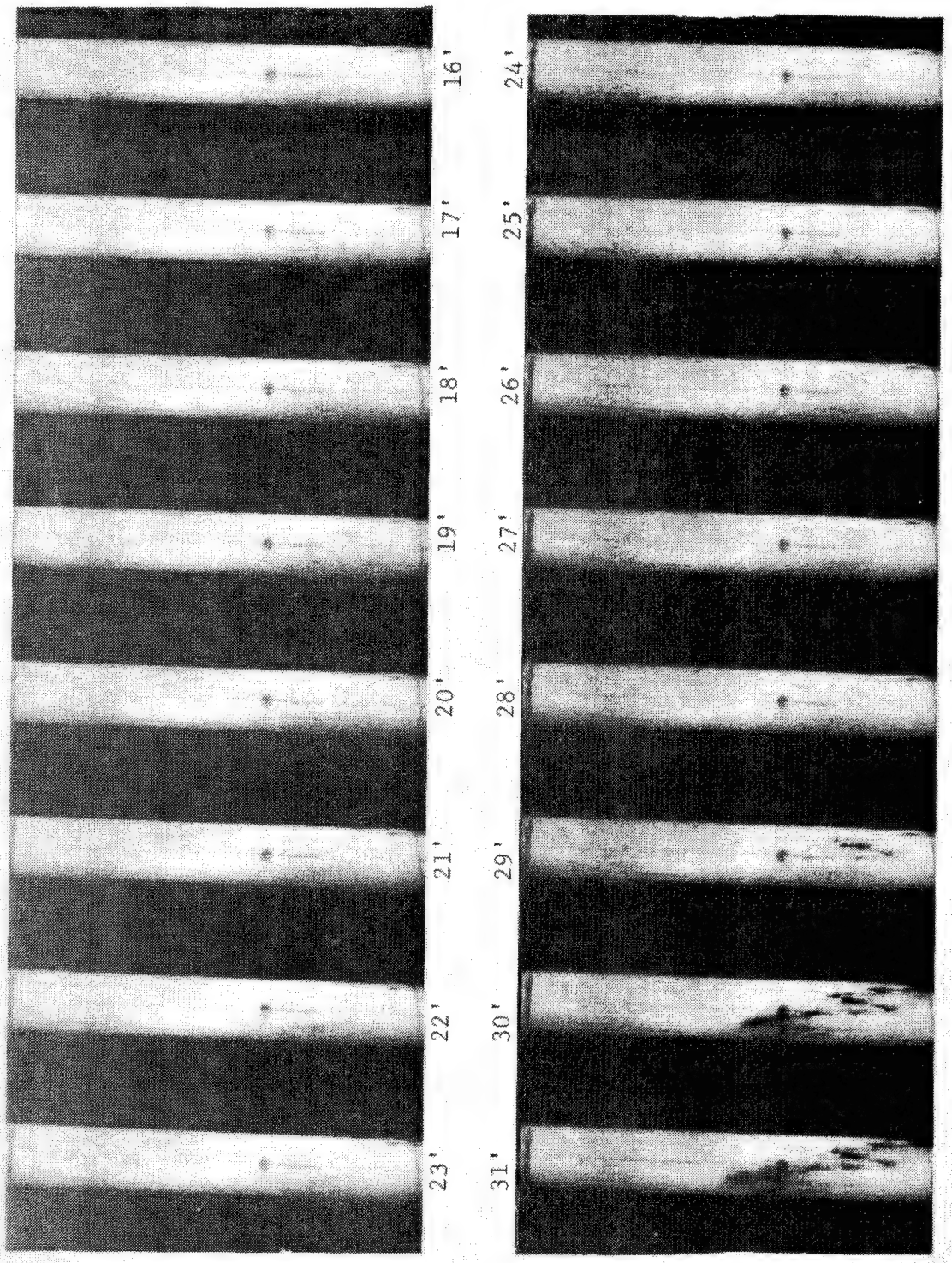

Fig. 15b Continued

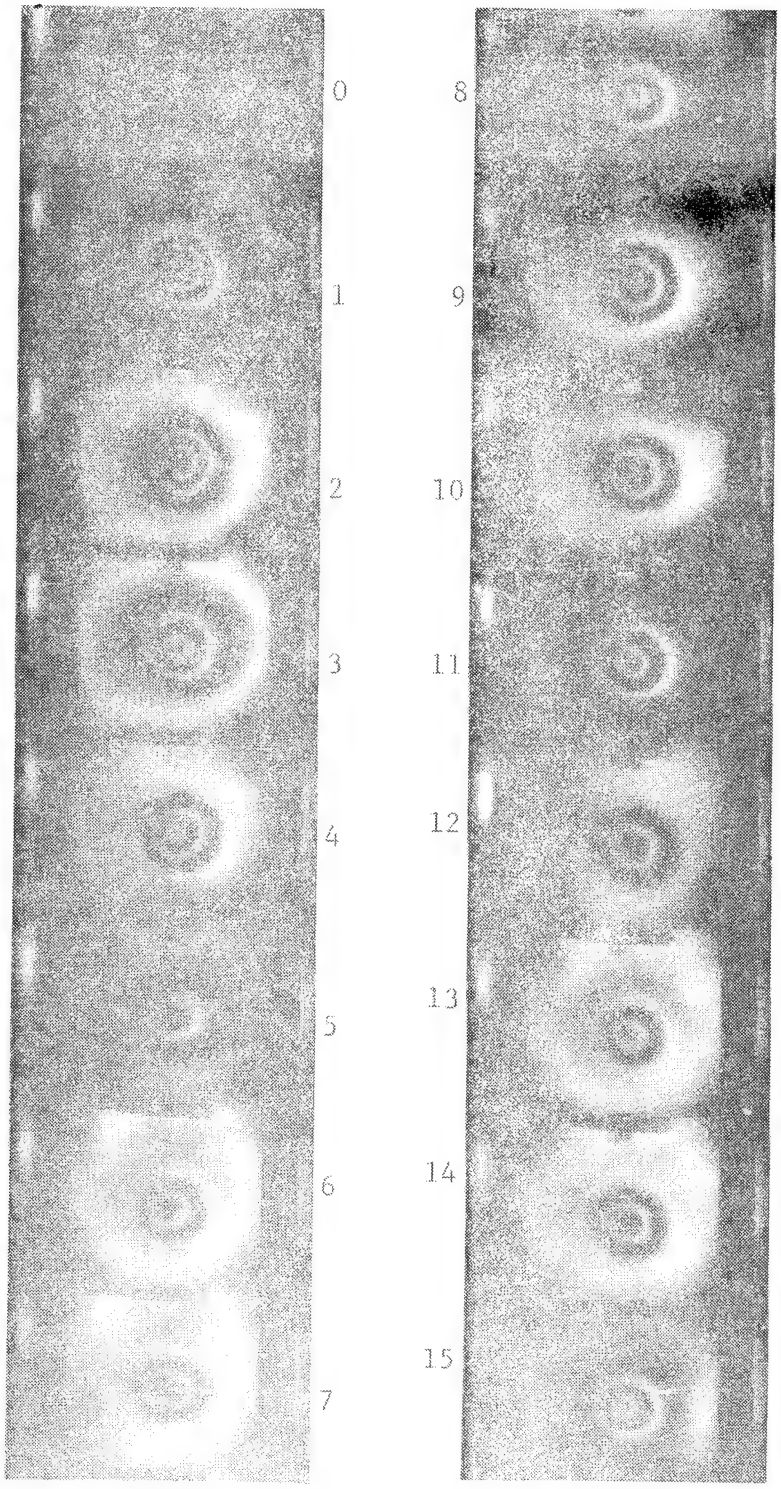

Fig. 16a Test Panel AB-3, 18,400 frames/sec

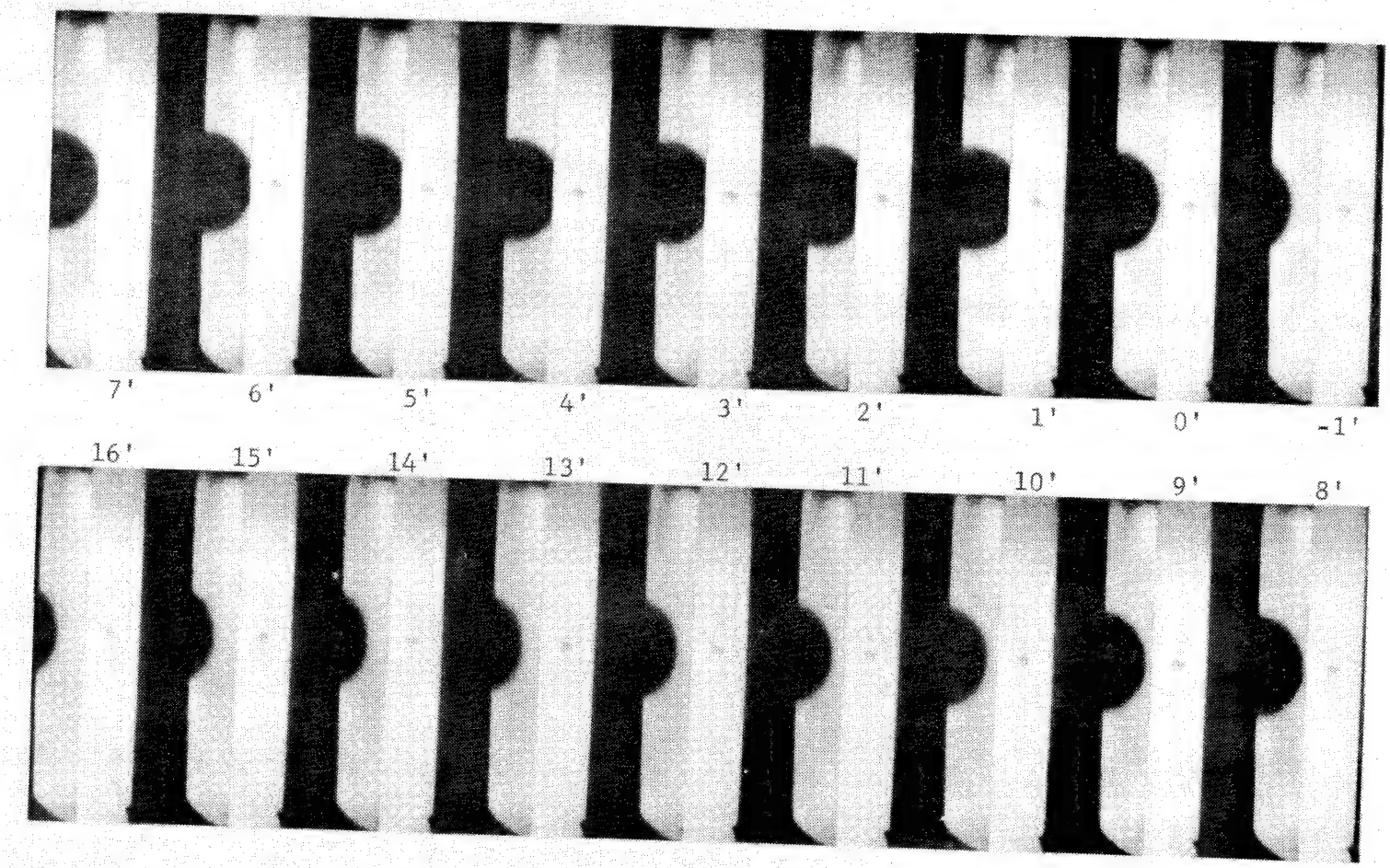

Fig. 16b Test Panel AB-3, 19,800 frames/sec.

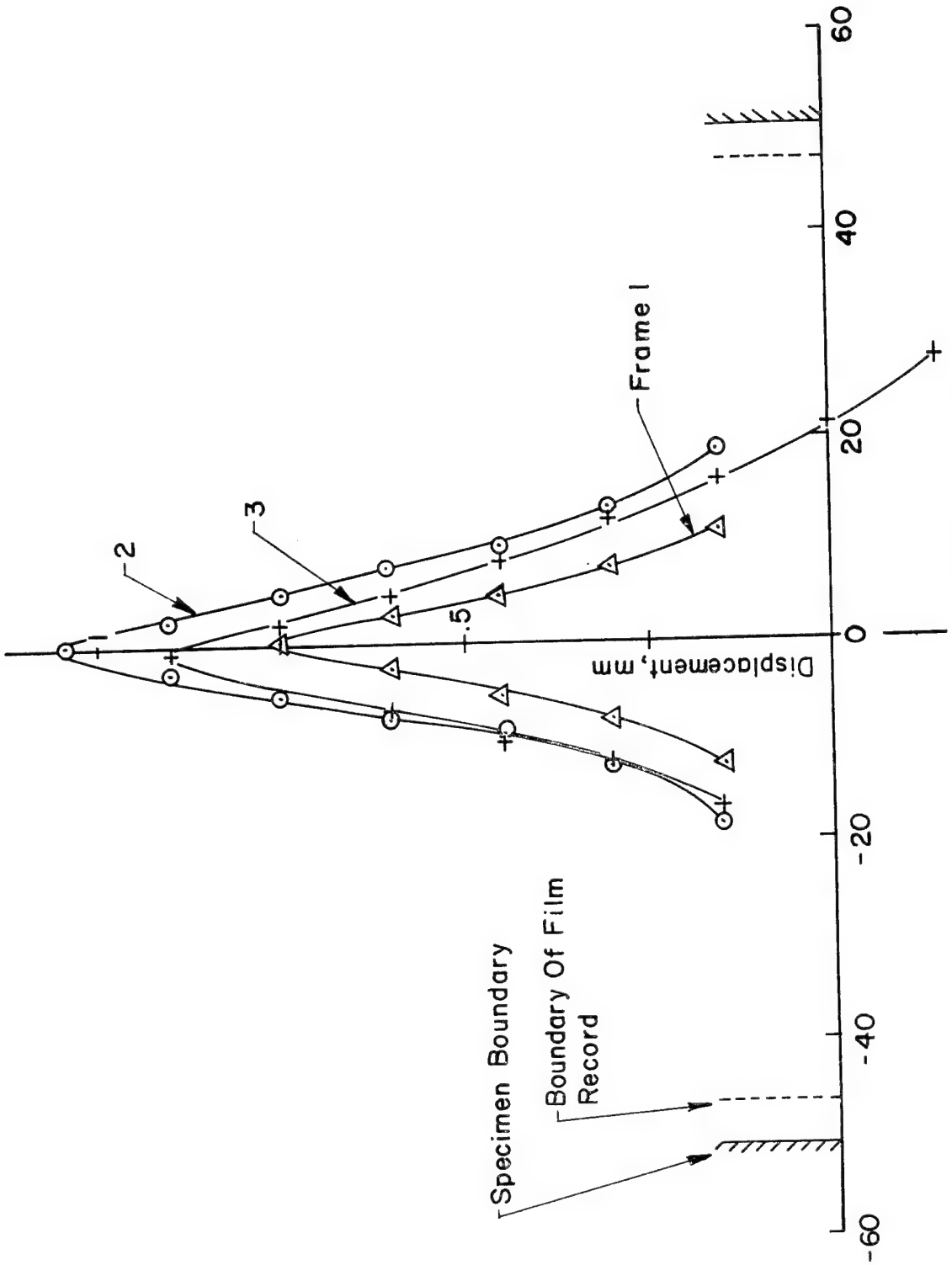

FIG. 17 TEST PANEL B-9 OUT OF PLANE DISPLACEMENT ALONG SPECIMEN WIDTH
(time interval between frames – 50.25 μs)

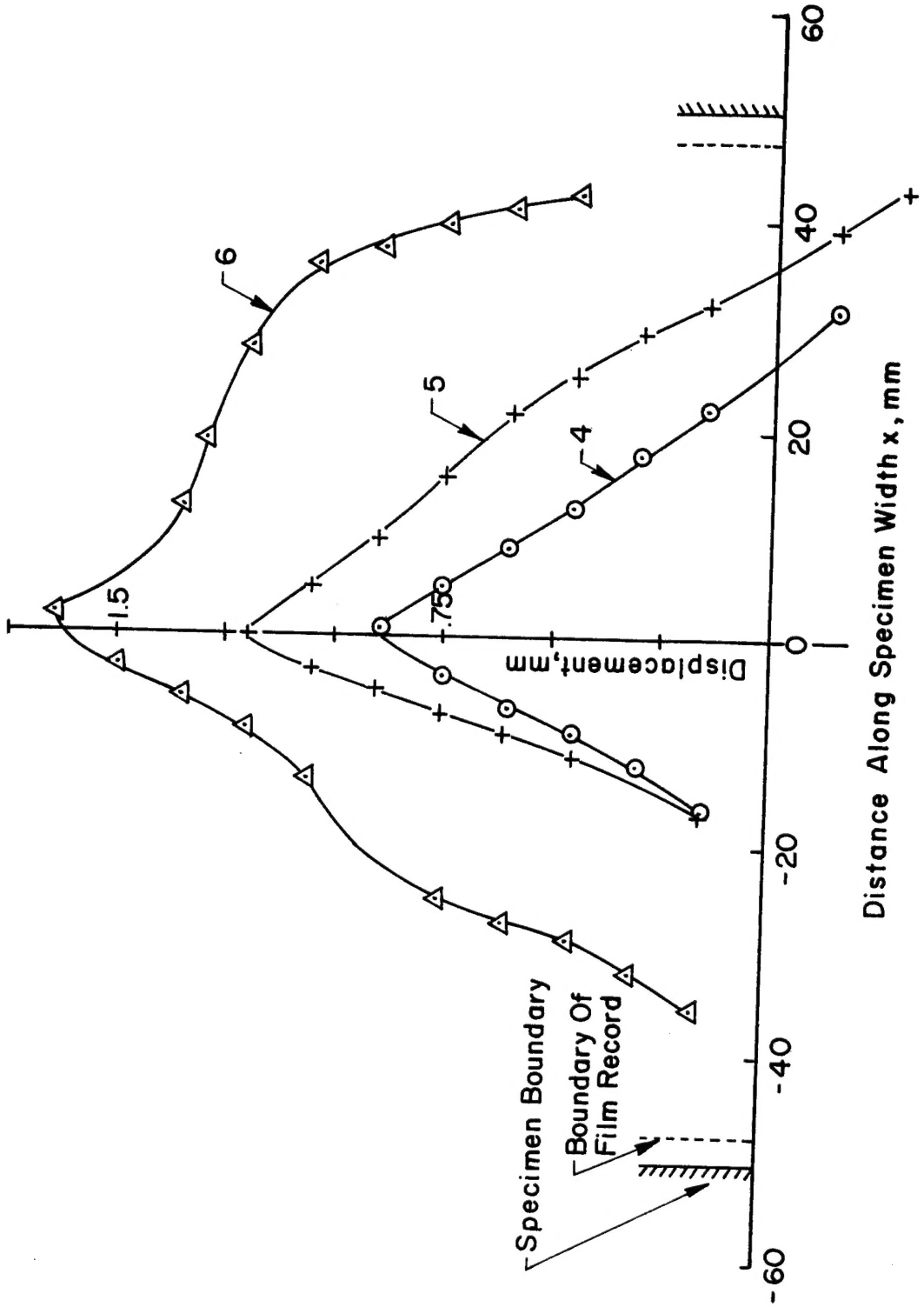
Distance Along Specimen Width x, mm
Displacement, mm
Specimen Boundary
Boundary Of Film Record
6
5
4
1.5
.75
60
40
20
0
-20
-40
-60

FIG. 17 Cont.

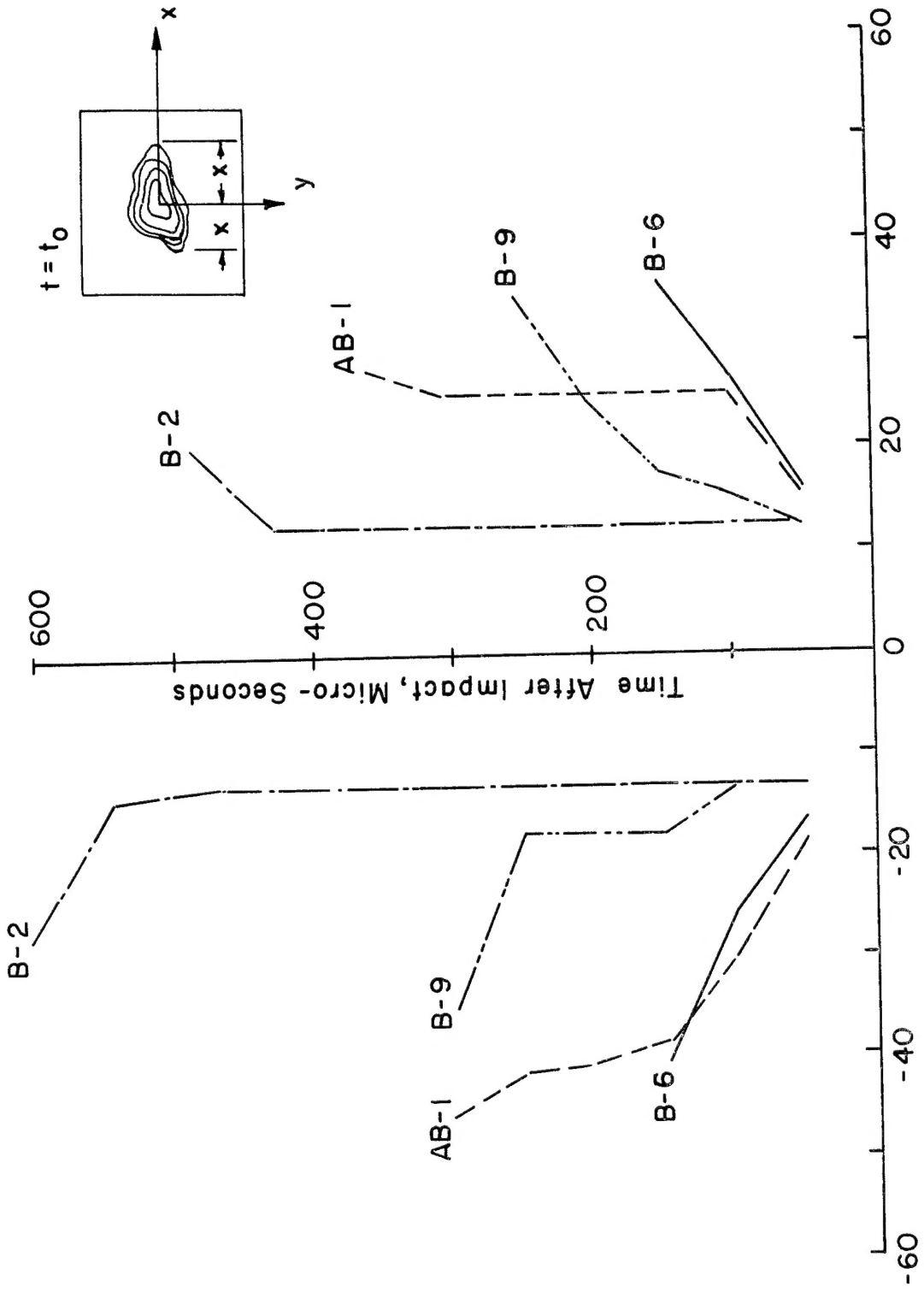

FIG. 18 DELAMINATION TIP POSITION ALONG PANEL WIDTH AS FUNCTION OF TIME

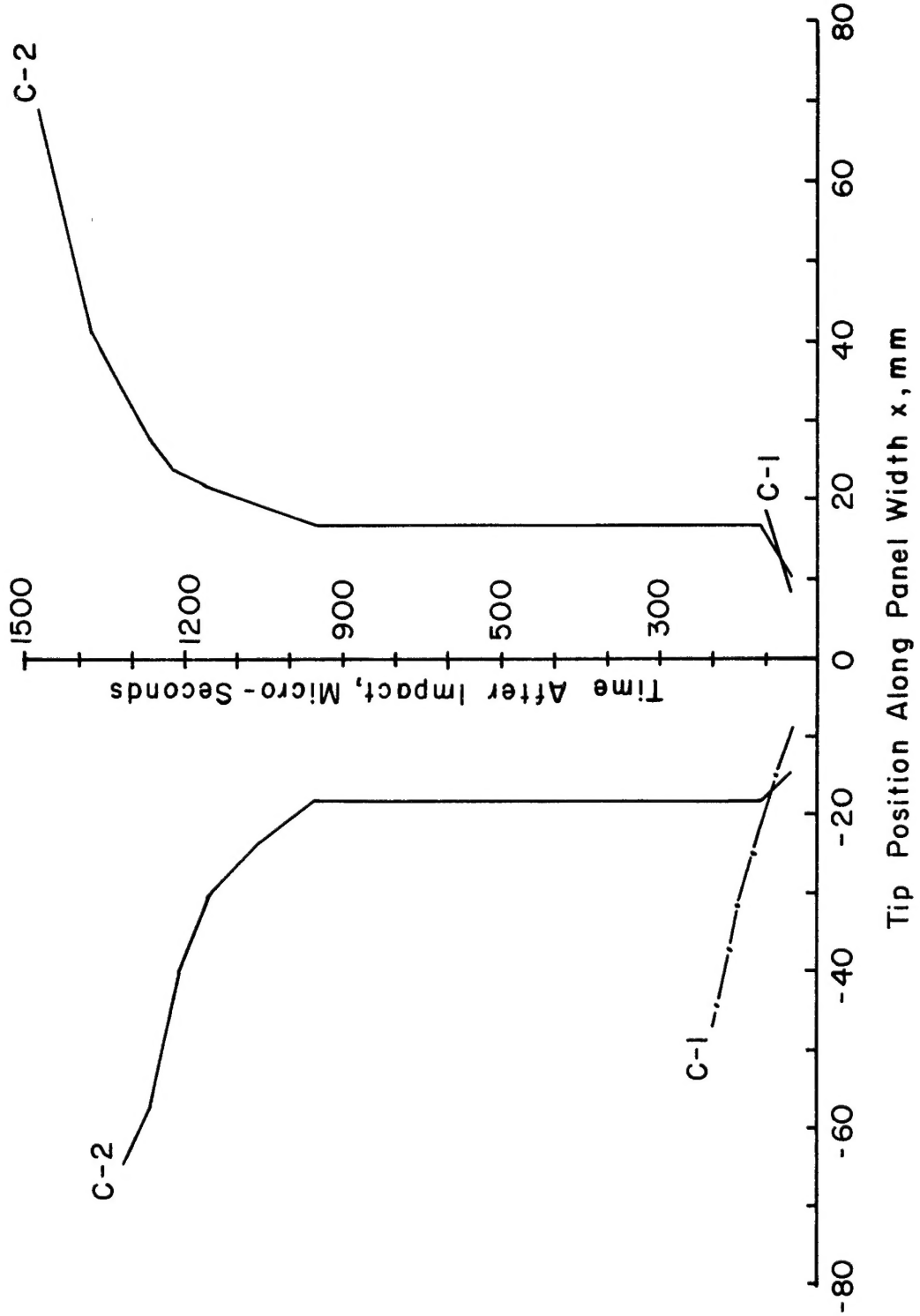
C-2
C-1
1500
1200
900
500
300
Time After Impact, Micro-Seconds
80
60
40
20
0
-20
-40
-60
-80
Tip Position Along Panel Width x, mm
C-2
C-1

FIG. 18 Cont.

1. Report No.	2. Government Accession No.	3. Recipient's Catalog No.
NASA CR-159261		

4. Title and Subtitle	5. Report Date
VISUALIZATION OF IMPACT DAMAGE OF COMPOSITE PLATES BY MEANS OF THE MOIRÉ TECHNIQUE	April 1980
	6. Performing Organization Code

7. Author(s)	8. Performing Organization Report No.
W.G. Knauss, C.D. Babcock, and H. Chai	SM 79-9
	10. Work Unit No.

9. Performing Organization Name and Address	11. Contract or Grant No.
California Institute of Technology Pasadena, CA 91125	NSG-1483
	13. Type of Report and Period Covered

12. Sponsoring Agency Name and Address	13. Type of Report and Period Covered
National Aeronautics and Space Administration Washington, DC 20546	Contractor Report
	14. Sponsoring Agency Code

15. Supplementary Notes

Langley Technical Monitor: Dr. James H. Starnes, Jr.
Topical Report

16. Abstract

The results of a program to determine the phenomenological aspects of the propagation damage due to low velocity impact on heavily loaded graphite-epoxy composite laminates are described. The main tool of this investigation is high speed photography coupled with the moiré fringe technique. High speed moiré motion records of the impacted specimens are presented.

The test results provide information on the time scale and sequence of the failure process. While the generation of the initial damage cannot always be separated temporally from the spreading of the damage, the latter takes place on the average with a speed on the order of 200 m/sec.

17. Key Words (Suggested by Author(s))	18. Distribution Statement
Composite Compression Impact Damage	Unclassified - Unlimited Subject Category 39

19. Security Classif. (of this report)	20. Security Classif. (of this page)	21. No. of Pages	22. Price*
Unclassified	Unclassified	52	

* For sale by the National Technical Information Service, Springfield, Virginia 22161